NOAA Technical Memorandum ERL GLERL-16

A GENERAL CIRCULATION MODEL FOR LAKES

J. C. K. Huang

Great Lakes Environmental Research Laboratory
Ann Arbor, Michigan
August 1977

CONTENTS

iii

FIGURES

TABLE

iv

A GENERAL CIRCULATION MODEL FOR LAKES*

J. C. K. Huang

A time-dependent, three-dimensional numerical dynamic model
for a large lake, possessing the actual coastal configuration and
bottom topography of the lake and with a flexible number of verti-
cal layers, has been developed to simulate the organized water
motion and temperature structure throughout the annual cycle of
the lake and to understand the physical nature of the lake in
response to atmospheric forcing.

The model is based on time integration of the finite dif-
ference form of the primitive equations. Fresh water density
is approximated as a quadratic function of temperature. Lake
circulation is driven by imposed meteorological conditions.
The flux form of a mass, momentum, and energy conservation
numerical scheme is used for the finite difference equations
of the model. Based on the simulated energetics, the major
physical processes and dominant dynamic mechanisms responsible
for variations and fluctuations in lake properties are
identified.

Test runs have been carried out with the geometry and
bathymetry of Lake Ontario on a 5-km grid with four vertical
layers. Reported here are two cases with surface winds and
heat similar to the mean state of July and November. Results
show that the whole lake response is dominantly barotropic
and gradually becomes baroclinic. The vertically integrated
stream functions for southwest and northeast winds form a
two-gyre circulation pattern. There is an elongated anticy-
clonic gyre in the north and a cyclonic one in the south in
the former cast?, and reversed circulation in the latter case.
The surface layer currents show strong coastal jets, about
10 cm/s, in the direction of the wind in the shallow regions
and a weaker return flow in the middle of the lake. Lower
layers contain return flows along the bathymetry of the deep
lake to balance the pressure gradient due to the wind set-up.
Some comparisons are made with International Field Year for
the Great Lakes data and further improvements for the model
are pointed out.

1. INTRODUCTION

The Laurentian Great Lakes constitute the largest body of fresh water in
the world and have long been considered the inland "oceans" of the North
American continent. In spite of various differences between the properties
of oceans and those of fresh-water lakes, general physical phenomena in the

---

two are quite similar. The special characteristics of a fresh-water lake
with negligible tidal effect and the more tractable boundary conditions make
the lake an ideal, if huge, hydrodynamic laboratory. In addition to the
scientific interest in limnological and oceanographic studies as a shallow
sea, the economic wealth of these water resources are invaluable. In 1972,
the International Field Year for the Great Lakes (IFYGL) was initiated as the
first essential step toward a coherent understanding of one of the "model
oceans" - Lake Ontario.

The rapid advance of modem computer technology had made it possible to
numerically simulate large-scale atmospheric and oceanic phenomena. when
these numerical simulations have been properly tuned to the observational
data, they yield realistic and physically meaningful results and become power-
ful tools for dynamic studies. The Great Lakes Environmental Research Labora-
tory (GLERL) research program affords a unique opportunity to perform large-
scale dynamic modeling of the lake-atmosphere system in the Great Lakes Basin
with the central objective of improving the environmental information concern-
ing phenomena and processes of the Great Lakes and of developing better envi-
ronmental service tools to the community. Lake-scale modeling in such a pro-
gram will set the stage for more local small-scale process studies to indicate
those regions of maximum sensitivity and/or variability in the lake and to
show the dynamic relationships between diverse parts of the lake basin. Above
all, the lake-scale model is the fundamental simulation for comparisons with
field observations for realistic tuning; hence it can provide the time-depend-
ent, evolutionary climatology for all the lakes. Following the methodology
and technology advanced in the hydrodynamical and thermodynamical models in
the atmospheric and oceanic sciences, we have developed the lake simulation
model to achieve the aforementioned objectives.

Numerical studies of lake dynamics in a realistic basin are relatively
recent. In 1958, Platzman developed a two-dimensional homogeneous model to
investigate the water level fluctuations in southern Lake Michigan caused by
the passage of an intense and fast-moving squall line. He later applied the
storm surge model to Lake Erie (Platzman 1963, 1965). Since then, many one-
dimensional and two-dimensional models have also been developed. Pandolfo
and Jacobs (1972) studied the air-lake interactions by a vertical one-dimen-
sional model. Rao and Murty (1970) employed a linear, homogeneous model for
steady state wind-driven circulations in Lake Ontario. Paskausky (1971) did
a similar study for the winter season. The initiation of the IFYGL program
has led to a more complete approach in developing three-dimensional models
(e.g., Gedney and Lick, 1972; Leendertse et al., 1973; Simons, 1973; Baba,
1974; Bennett, 1976). Following the numerical scheme advanced in ocean model-
ing (e.g., Bryan, 1969; Gates, 1968), Simons (1973) developed a rather advanced
multilayered model for Lake Ontario. Simon's model took most major physical
processes into consideration, including the free-surface dynamics. He later
dropped the nonlinear processes of momentum in the model. The free-surface
displacement was predicted in his model from a vertically integrated one-
layer model, which undoubtedly had to take very short time steps due to the
existence of the surface gravity wave. The computational efficiency of the
model was improved by eliminating the free surface terms in his multilayered
internal flow equations, which then could take a longer time step. However,
the integrated transport had to be used to update the internal flow and vice

versa. The repeated back and forth corrections between the integrated trans-
port and the layered transports are still computationally lengthy. Neverthe-
less, Simon's model has been calibrated to the Lake Ontario phenomena and
has achieved considerable accuracy in simulating the circulation pattern dur-
ing certain periods of IFYGL.

The lake circulation model we have developed takes all major physical
processes into account, including the nonlinear effects and the horizontal
viscous effects, with a rigid lid approximation for computational efficiency.
Based on internal wave theory (Munk and Phillips, 1968), the internal mode
in the lake is essentially unaffected by assuming the lake surface is a
balanced surface where the vertical velocity is null. The space-staggered
grids and the energy-conserving finite-difference schemes adopted in this
model follow those in the University of California at Los Angeles (UCLA)
atmospheric general circulation model (Gates et al., 1971) and are similar
to the ones used in ocean circulation models (Huang, 1973; Haney, 1974).
The simplified version of the Arakawa scheme (Arakawa, 1966) adopted in
the model conserves not only mass, momentum, and kinetic energy but also,
after a slight modification, other quadratic properties. The upper boundary
condition of the present model is specified in a manner coupling the dynamics
to the observed atmospheric parameters, thus imposing a closer-to-realistic
atmosphere-lake interaction. The downward heat flux into the top layer of
the lake is determined by the balance of all terms in the atmospheric heat
budget equation. The effect of atmospheric stability near the air-water
interface is also taken into consideration. This paper describes the numer-
ical model, based on primitive equations in which the mean motion and tem-
perature field in the lake are assumed to be produced by surface wind stress
and atmospheric heating, and shows some preliminary results from Lake Ontario
simulations.

2. FORMULATION

The formulation of the model is based on primitive equations relative
to a geographic coordinate system on the surface of the earth (in latitudes
and longitudes for convenience). In the lake, the Boussinesq approximation
is generally valid because the actual density distribution differs only
slightly from the motionless reference state in which the entropy is constant
and the vertical scale of motion is small compared with the scale height.
Variations in the pressure on a fluid element in the lake are predominately
the result of variations in water depth which justify the use of hydrostatic
approximation. To simulate subgrid scale diffusion of momentum and heat, the
eddy viscosities and diffusivities have been parameterized from implicit treat-
ment of stresses and turbulent mixing due to the small-scale motions.

2.1 The Physical Model

Let $\mathbb{V}$ be the horizontal velocity; then under the above assumptions, the

3

governing equation of motion is

$$\frac{d\mathbb{V}}{dt} = -\frac{1}{\rho_0}\nabla p - 2\Omega\mathbb{X}\mathbb{V} + \mathbb{F},\tag{1}$$

where Ω is the earth rotation vector, $\mathbb{F}$ is the horizontal component of frictional force per unit mass, and all other symbols and nomenclatures are as listed in Appendix A. Note that the left hand side of (1) is the Eulerian derivative, including all the nonlinear advective terms as follows:

$$\frac{d\mathbb{V}}{dt} \equiv \frac{\partial\mathbb{V}}{\partial t} + \nabla\cdot(\mathbb{V}\mathbb{V}) + \frac{\partial w\mathbb{V}}{\partial z}.\tag{2}$$

An approximate form of frictional force F is written

$$\mathbb{F} = \nu\nabla^2\mathbb{V} + \frac{\partial}{\partial z}\left(\nu_1\frac{\partial\mathbb{V}}{\partial z}\right),\tag{3}$$

where ν and ν_1 are the lateral and the vertical kinematic eddy viscosity, respectively. Values used in the model are listed in Table 1. Though variable nonlinear viscosity formulation will be attempted at a later stage, a quasi-linear viscosity proportional to the four-thirds power of the horizontal grid size (Leith, 1968) has been used in the present model for the parameterization of subgrid scale motions.

Under the hydrostatic assumption, the pressure at any level in the lake can be uniquely determined by vertical integration of the hydrostatic equation, provided the variation of the free surface with respect to the mean reference lake surface (i.e., $z = 0$) and the atmospheric pressure there are known. The hydrostatic equation is

$$\frac{\partial p}{\partial z} = -\rho g.\tag{4}$$

Then the pressure at any depth may be written

$$p(z) = p_a + \int_z^\xi \rho g\,dz = p_s + \int_z^0 \rho g\,dz,\tag{5}$$

where ξ is the height of free surface and P_s is the pressure at the balanced lake surface.

4

Table 1. Values of Constants Used in the Model

Constants	Symbol	Value	Unit
Earth rotation rate	Ω	2π	Day^{-1}
Specific heat of water	C_p	1	CAL gm^{-1} °C^{-1}
Specific heat of air	C_a	0.24	CAL gm^{-1} °C^{-1}
Reference temperature	T_o	4	°C
Reference density of water	ρ_o	1	gm cm^{-3}
Mean density of air	ρ_a	1.23×10^{-3}	gm cm^{-3}
Proportional constant for density anomaly	b	6.6×10^{-6}	°C^{-2}
Basic lateral eddy viscosity	ν	1.5×10^{6}	cm^2 s^{-1}
Basic vertical eddy viscosity	ν_1	5	cm^2 s^{-1}
Basic lateral eddy diffusivity	κ	10^6	cm^2 s^{-1}
Basic vertical eddy diffusivity	κ_1	1	cm^2 s^{-1}
Constants in the bulk Richardson number	β_v, β_T	4.7	
Drag coefficient of momentum under neutral stability	$(C_D)_N$	2.5×10^{-3}	cgs
Exchange coefficients of heat and water under neutral stability	(C_H), $(C_E)_N$	$(C_D)_N(0.74)^{-1}$	cgs
Constants	b_1, b_2	52.9, 53.2 cgs	
Gravitational constant	g	981	cm s^{-2}
Empirical constant	Z_{10}	10^3	cm
Empirical constant	T_{vo}	290	°K
Bottom frictional coefficient	C_b	2.5×10^{-3}	cgs
Latent heat of evaporation	L	595	cal gm^{-1}
Unit time step	At	1.5	hrs
Stability factor for Coriolis term	a	0.55	
Radius of the earth	a	6371.2	km
Marginal lapse rate of density	ϵ_ρ	10^{-8}	s^{-2}
Marginal stable criterion for temperature	ϵ_T	10^{-5}	°C cm^{-1}

The equation of state will yield sufficiently accurate density variation from a quadratic approximation involving the difference between the ambient temperature and the temperature of maximum density of the fresh water

$$\rho = 1 - b (T - T_o)^2, \tag{6}$$

where b is a proportional constant as shown in Table 1. Note that the second part of the right hand of (6) is the density anomaly relative to the reference density (Simons, 1973), which contributes to the internal pressure distribution affecting the baroclinic current. The continuity equation for incompressible fluid is

$$\nabla \cdot \mathbb{V} + \frac{\partial w}{\partial z} = 0. \tag{7}$$

The tendency equation for the temperature is obtained from the conservation of heat energy

$$\frac{dT}{dt} = \frac{Q}{\rho_o C_p}, \tag{8}$$

where the rate of heating Q is given by

$$Q = C_p \left[\kappa \nabla^2 T + \frac{1}{\delta} \frac{\partial}{\partial z} \left(\kappa_1 \frac{\partial T}{\partial z} \right) \right] \tag{9}$$

and κ and κ_1 are the diffusivities as shown in Table 1. Note that, although in most cases the vertical column of the lake water is stable, an unstable configuration due to the vertical density stratification can occur at any level and may cause vertical mixing in the lake. Since the instability in natural phenomena lasts only a short period of time, the simplest treatment for the hydrostatic instability is an instantaneous convective density adjustment mechanism. Whenever instability is detected between layers, a quasi-homogeneous mixed density of marginal stable lapse rate is assumed for all unstable adjacent layers. The coefficient δ, defined by

$$\delta = \begin{pmatrix} 1 \\ 0 \end{pmatrix} \quad \text{for } \frac{\partial T}{\partial z} \begin{pmatrix} > \\ < \end{pmatrix} 0, \tag{10}$$

performs such a function of convective adjustment.

2.2 Boundary Conditions

The boundary conditions at the lake surface $(z = 0)$ are

$$w = 0, \qquad \frac{\partial w}{\partial z} = \frac{\tau_s}{\rho_o \nu_1}, \qquad \frac{\partial T}{\partial z} = \frac{Q_S}{C_p \rho_o \kappa_1}, \qquad (11)$$

where τ_s is the wind stress and Q_s is the downward heat flux at the surface. The vertical velocity is assumed zero and the stress as well as the heat are balanced at the atmosphere/lake interface. The wind stress and the heat flux are functions of atmospheric parameters coupling with the lake surface state. All atmospheric forcing functions will be discussed in the next section.

The boundary conditions at the lake bottom $z = -D(\lambda, \phi)$ are

$$w = -V \cdot \nabla D, \qquad \frac{\partial w}{\partial z} = \frac{\tau_b}{\rho_o \nu_1}, \qquad \frac{\partial T}{\partial z} = 0 \qquad (12)$$

The flow is required to parallel the bottom slope and the bottom stress is computed from a simple friction law,

$$\tau_b = \rho_o C_b \mid V_b \mid V_b, \qquad (13)$$

where V_b is the flow velocity near the bottom. The bottom friction coefficient C_b is an empirical constant as shown in Table 1. The thermal heat flux through the bottom is neglected.

At all lateral boundaries, no slip and no flux of heat conditions are imposed.

2.3 Atmospheric Forcing Functions

In the large-scale model, the organized mean motion and the density structure in the lake basin are products of the surface wind stress and the atmospheric heating. The transfer of momentum at the atmosphere-lake interface depends on the drag coefficient, which is a function of the state of the lake surface. The surface heat flux depends greatly on the coupled temperature difference between the atmosphere and the lake. Since the atmospheric conditions imposed as the upper boundary conditions of the lake are specified, equivalent atmospheric processes together with the prescribed atmospheric parameter from observational data must be used to approximate the surface heat flux.

The net downward heat flux, according to the heat balance equation, can be written as

$$Q_S = Q_I - Q_B - Q_H - Q_E, \tag{14}$$

where Q_I is the net downward flux of solar insolation and Q_B, Q_H, Q_E are upward fluxes of long wave radiation, sensible heat, and latent heat, respectively, as defined in Table 1. Table 1 also contains all other notations used in the following formulas.

The solar radiation flux can be calculated from a simplified formula with empirical constants obtained from the atmospheric climatology (London, 1957; Vonder Haar and Hanson, 1969) as

$$Q_I = 0.95 \, Q_o \, (0.74 - 0.6 \, N_c). \tag{15}$$

The net upward infrared heat flux is calculated from (Johnson et al., 1958)

$$Q_B = 0.985 \, CT_S^4 \, (0.39 - 0.05 \, e_a^{1/2}) \, (1 - 0.6 \, N_c^2). \tag{16}$$

The sensible and latent heat are computed from

$$Q_H = \rho_a \, C_H \, C_a \, | \, V_a \, | \, (T_s - T_a) \tag{17}$$

and

$$Q_L = \rho_a \, C_E \, L \, | \, V_a \, | \, (q_s - q_a), \tag{18}$$

where $| \, V_a \, |$ is the wind speed at 10" above the surface. The specific humidity is related to the vapor pressure by

$$q = \frac{0.622}{P_a} \, e, \tag{19}$$

where P_a is the mean atmospheric surface pressure. The saturated vapor pressure at the lake surface temperature can be calculated from the Clausius-Clapeyron equation (Hess, 1959),

$$e_s = 10.0 \ \exp\left(\frac{9.4051 - 2353}{T_s}\right). \tag{20}$$

The momentum flux at the atmosphere-lake interface is expressed as the surface wind stresses,

$$\tau_s = \rho_a \ C_D \ | \ V_a \ | \ V_a, \tag{21}$$

where V_a is the wind velocity. Following Deardorff (1968) and using data from Businger et al. (1971), the exchange coefficients of heat, water, and momentum are functions of atmospheric stability as

$$C_D = (C_D)_N \ \exp(-2 \ \beta_v \ R)$$

for stable cases (R > 0) and

$$C_H = C_E = (C_H)_N \ \exp\left[- (\beta_v + \beta_T) \ RI\right] \tag{22a}$$

$$C_D = (C_D)_N \ \left[1 + \frac{7}{b_1} \ln \ (1 - b_1 R)\right]$$

for unstable cases (R < 0),

$$C_H = C_E = (C_H)_N \ \left[1 + \frac{11}{b_2} \ln \ (1 - b_2 R)\right] \tag{22b}$$

where R is the bulk Richardson number (a parameter to measure the stability of the atmosphere) and

$$R = \frac{g Z_{10}}{T_{vo} W_a^2} \ \left[(T_a - T_s) + 0.38 \ T_a \frac{(e_a - e_s)}{P}\right], \tag{23}$$

where β_v, β_T, $(C_D)_N$, b_1, b_2, Z_{10}, and T_{vo} are constants (Businger et al., 1971) as listed in Table 1. The coefficient of water particle exchange is assumed to be the same as that of heat exchange. Note that the above empirical formulas are in general valid in the lower atmospheric boundary layers (Businger et al., 1971). However, there are no direct observational data available for their verification in the Great Lakes region. In our studies,

all values of atmospheric parameters (i.e., T_a, e_a, N_c, V_a, τ_s) are compiled from the IFYGL data bank.

2.4 Integral Constraints

The following integral constraints are derived from the differential equations and are preserved in the latter finite difference equations.

2.4.1 Conservation of Mass

Mass conservation can be obtained from the continuity equation (7) and boundary conditions (11) and **(12)**, which lead to

$$\nabla \cdot \int_{-D}^{0} \mathbb{W} \, dz = 0 \quad \text{or} \quad \int_{V} \nabla \cdot \mathbb{W} \, dV = 0, \tag{24}$$

where $D(\lambda, \phi)$ is the depth of the water column and V denotes the integration over the entire lake domain.

2.4.2 Conservation of Momentum

The momentum equation **(1)**, together with the boundary conditions of zero normal flows at all lateral boundaries, the zero vertical velocity at the balanced upper surface, and the bottom flow along the slope yields

$$\frac{\partial}{\partial t} I, \ \rho_0 \mathbb{V} dV = \int_{V} (-\nabla P - 2\Omega X \ \rho_0 \mathbb{W} + \mathbb{F}) \, dV. \tag{25}$$

2.4.3 Conservation of Moments of Temperature

The temperature prediction equation **(8)**, together with the insulation conditions on all solid boundaries, leads to

$$\frac{\partial}{\partial t} \int_{V} \frac{T^m}{m} \, dV = \int_{V} \frac{Q}{\rho_o C_p} T^{m-1} \, dV, \tag{26}$$

where m is an integer equal to, or greater than, 1.

2.4.4 Conservation of Energy

For the conservation of kinetic energy, we take the dot product of (1) with \V and employ the hydrostatic approximation (4). After applying all

boundary conditions, the result is

$$\frac{\partial}{\partial t} \int_V \rho_o \frac{V^2}{2} \, dV = \int_V [-\rho g w + \rho_o (V \cdot F)] \, dV. \tag{27}$$

The conservation of potential energy is based on the thermodynamic equation (8) and the equation of state (6). Multiplying $-2b\rho_o (T - T_o)$ to (8) and integrating over the whole lake yields

$$\frac{\partial}{\partial t} \int_V \rho g (Z + D) \, dV = \int_V \left[\rho g w - 2bg (Z + D)(T - T_o) \frac{Q}{C_p} \right] dV. \tag{28}$$

3. METHOD OF SOLUTION

Equations (1), (4), (6), (7), and (8) constitute a closed system for the six dependent variables u, v, w, P, p, and T, among which u, v, and T are prognostic variables and w, P, and p are diagnostic variables. The boundary condition (12) implies that the lake surface is not a free surface but rather a balanced surface where the vertical velocity is null. With this rigid lid approximation (Bryan, 1969), the external inertio-gravity waves are filtered out with essentially no effect on the internal modes. The stability criterion for the time step in the lake model can be based on the internal wave, which is much slower than the surface wave. This increases the allowable time step to a much greater value; this is preferable in a general circulation model.

The exclusion of the kinematic surface variation makes the surface pressure difficult to calculate. This implies that the barotropic effect on current generation due to surface fluctuations cannot be explicitly obtained from (1) under the rigid lid approximation. Instead we compute the shear current (V') as a prognostic variable in (1) by substituting the vertically integrated hydrostatic equation for the pressure terms. The vertical mean current (V), on the other hand, is obtained from the stream function by solving the vorticity equation. The total velocity is, then, the combination of the vertical mean (barotropic) velocity and the deviation from the vertical mean shear current (baroclinic)

$$w = V + V'. \tag{29}$$

The surface and the bottom boundary conditions (11) and (12) on w permit us to define the vertically integrated stream function that satisfies the continuity equation as

$$\hat{V} = k \times \frac{1}{D} \nabla \psi, \tag{30}$$

11

where $\hat{k}$ is a unit vertical vector.

A predictive equation for ψ that does not include explicitly the surface pressure effect is obtained by taking the vertical mean and then the curl of (1). Applying the curl operator, defined as

$$\nabla_z \times (q, q^*) = \frac{1}{a \cos \phi}\left[\frac{\partial q^*}{\partial \lambda} - \frac{\partial}{\partial \phi}(q \cos \phi)\right],$$

to the vertical mean equation of (1) leads to

$$\left[\frac{\partial}{\partial x}\left(\frac{1}{D \cos \phi}\frac{\partial^2 \psi}{\partial \lambda \partial t}\right) + \frac{\partial}{\partial \phi}\left(\frac{\cos \phi}{D}\frac{\partial^2 \psi}{\partial \phi \partial t}\right)\right] = \frac{\partial}{\partial \lambda}\left(\frac{f}{D}\frac{\partial \psi}{\partial \phi}\right) - \frac{\partial}{\partial \phi}\left(\frac{f}{D}\frac{\partial \psi}{\partial \lambda}\right)$$

$$- \frac{\partial}{\partial \lambda}\left(\frac{g}{\rho_0}\widehat{\int_z^o \frac{\partial \rho}{\partial \phi}dz}\right) + \frac{\partial}{\partial \phi}\left(\frac{g}{\rho_0}\widehat{\int_z^o \frac{\partial \rho}{\partial \lambda}dz}\right) + a\frac{\partial}{\partial \lambda}(\hat{G}^* + \hat{F}^*)$$

$$- \frac{\partial}{\partial \phi}[a(\hat{G} + \hat{F})\cos \phi], \tag{31}$$

where G, G* are the components of the nonlinear effect

$$\mathbb{G} = -\nabla(\mathbb{V} \cdot \mathbb{V}) - \frac{\partial w \mathbb{V}}{\partial z} + \frac{uv}{a}\tan \phi \tag{32}$$

and F, F* the components of the frictional force as defined in (3).

The shear current ($\mathbb{V}'$) is predicted from the primitive equation (1) after subtracting the vertical mean part as

$$\frac{\partial \mathbb{V}'}{\partial t} = -\frac{1}{\rho_0}\nabla p' - 2\Omega \times \mathbb{V}' + \mathbb{G} + \mathbb{F} - (\hat{F} + \hat{G}), \tag{33}$$

where the superscript prime indicates the departure from its vertical mean.

Numerical solutions for the hydrothermodynamic system are obtained by computing in sequence the set of finite difference equations analogous to (4), (6), (7), (8), (30), and (31), together with appropriate boundary conditions described in the following sections. The shear current ($\mathbb{V}'$) and the stream function (ψ) are predicted from (33) and (31). The total current is then obtained according to (29), while the barotropic part of current ($\mathbb{V}$) is computed from ψ by (30). The vertical velocity (w) can be diagnostically obtained from (7). Then the temperature (T) is predicted from (8). The density (p) and the baroclinic part of the pressure (p') are also diagnostically computed from (6) and (4), respectively.

12

4. NUMERICAL SCHEME

The basic numerical scheme used in this model is essentially the same as in the North Pacific Ocean model (Huang, 1973). It is a modification of Haney's idealized ocean model (1974), quite similar to that of Bryan (1969). In the lake model, the actual configuration is taken into account by approximating 'the coastline coincident with the meridians or the latitude-circles passing through the nearest grid points as shown, for example, in Figure 1 for Lake Ontario. The origin of the coordinates is taken at the intersection of the mean lake surface with the most southern and the most western boundaries of the domain. The longitudinal coordinate has index i from $i = i_{j,k}$ on the western boundary to $i = I_{j,k}$ on the eastern boundary, and varies with the latitude and depth. Similarily, the latitudinal coordinate is indexed from $j = j_{i,k}$ at the southern boundary to $j = J_{i,k}$ at the northern boundary and varies with the longitude and depth. The maximum longitude, λ_m, corresponds to the most eastern boundary and the minimum longitude, λ_o, to the most western boundary of the surface layer in the operation domain. The maximum latitude, ϕ_m, corresponds to the most northern boundary and the minimum latitude, ϕ_o, to the most southern one. Since the origin is indexed as (1,1,1), the horizontal unit distances of finite difference are respectively,

$$\Delta \phi = \frac{\phi_m - \phi_o}{J_{max} - 1}$$

and

$$A A = \frac{\lambda_m - \lambda_o}{I_{max} - 1}, \tag{34}$$

where I_{max} and J_{max} are the maximum values of I and J, respectively.

The vertical coordinate z, indexed from k = 1 at the first depth level below the lake surface to $k = K_{i+1/2, j+1/2}$ at the last depth level above the bottom, is rather flexible. For the Lake Ontario model, we tentatively set four layers as shown in Figure 2. If Z_k denotes the depth in negative value of the kth level, the thicknesses between the levels are defined as

$$\Delta Z_{k+1/2} \equiv Z_{k-1} - Z_k, \quad k = 2 \ldots K_{i+1/2, j+1/2}$$
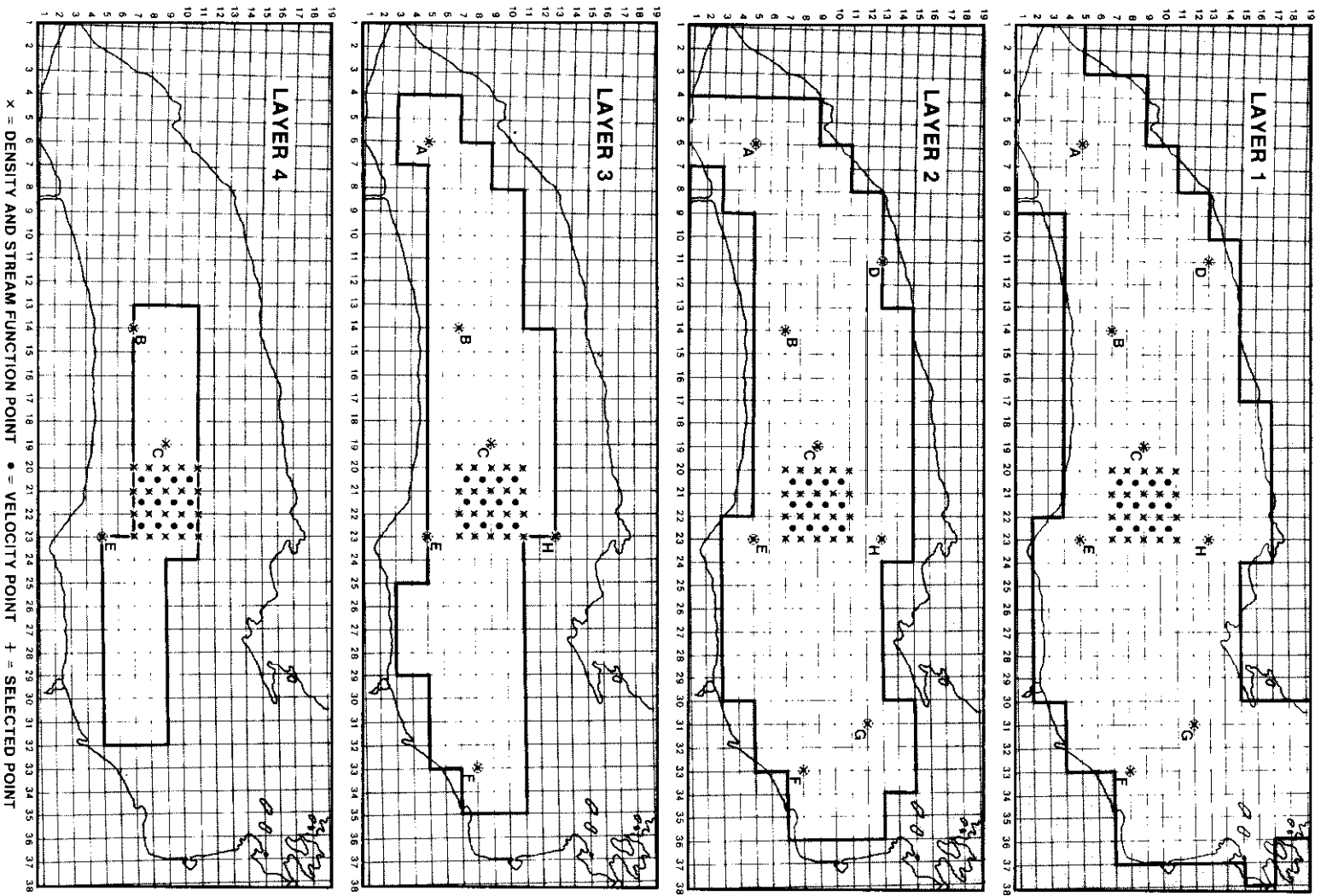
and

$$\Delta Z\frac{1}{2} \equiv -2 Z_1,$$

Figure 1. Configurations of the Lake Ontario Model at four different layer depths: K = 1 at 10 m, K = 2 at 30 m, K = 3 at 70 m, and K = 4 at 150 m.
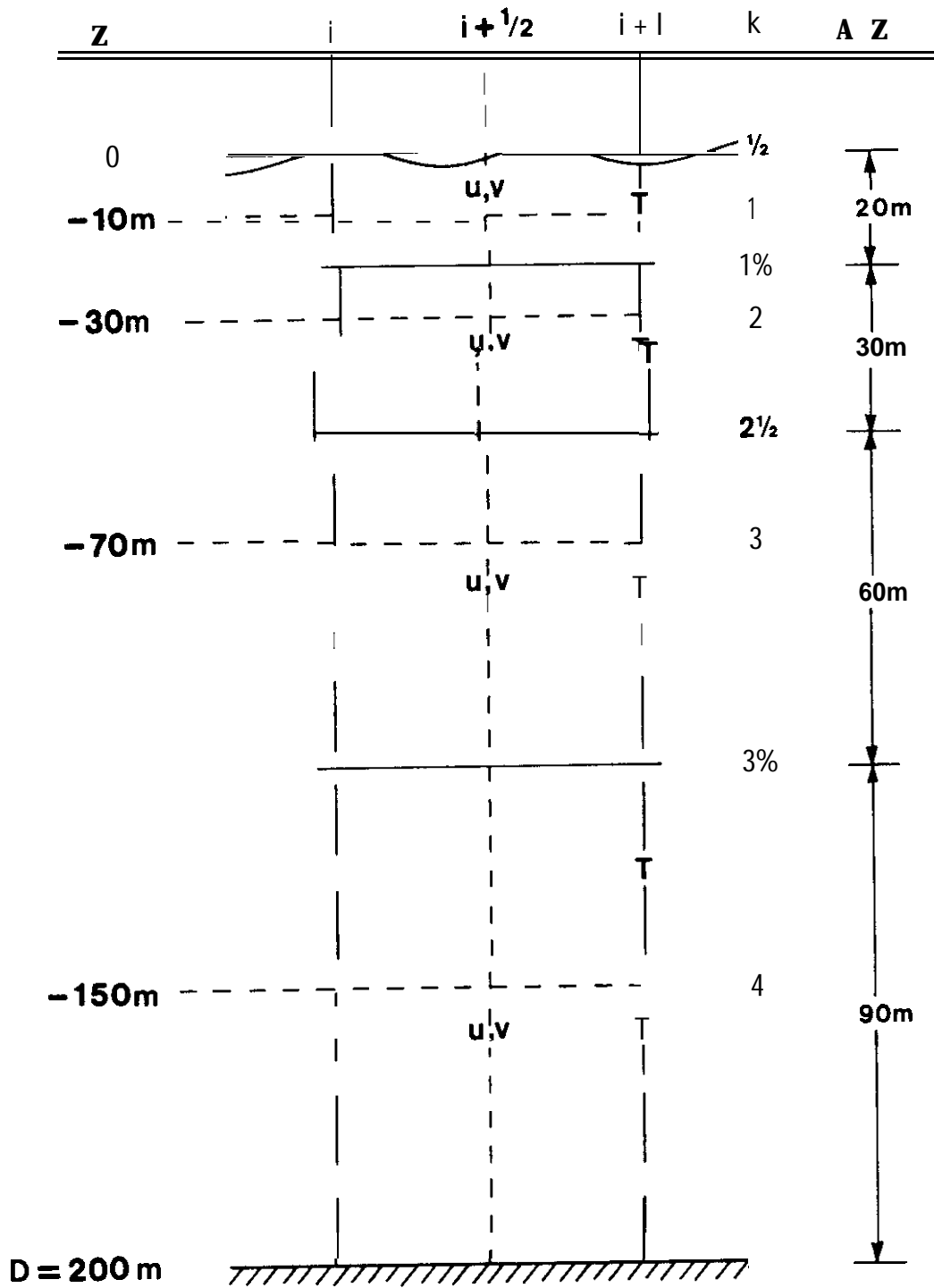
14

Figure 2. Vertical cross section of the velocity **and**
temperature points.

$$\Delta Z_{K_{i+1/2, j+1/2}} \equiv 2 (Z_{K_{i+1/2, j+1/2}} + D_{i+1/2, j+1/2}), \tag{35}$$

where $D_{i+1/2, j+1/2}$ is the upward total depth at the computational velocity point. The thickness of the kth level is defined as

$$\Delta Z_k = \frac{1}{2} (\Delta Z_{k-1/2} + \Delta Z_{k+1/2}), k = 1 \ldots K_{i+1/2, j+1/2}. \tag{36}$$

It is obvious that

$$D_{i+1/2, j+1/2} \equiv \sum_{k=1}^{K} \Delta Z_k. \tag{37}$$

Note that it is understood that subscripts of the maximum vertical index $K_{i+1/2, j+1/2}$ in the summation have been dropped for convenience.

The lake to be studied is approximated by a collection of computational boxes. both horizontal and vertical. We have denoted

$$\Delta X_{j'} \equiv a \cos \phi_{j'} \cdot \Delta \lambda$$

$$\Delta Y \equiv a \Delta \phi, \tag{38}$$

where the primed subscript may refer to the integer grid points or to the half integer grid points. Since the computation is carried out in flux form, the areas of a subvolumic box in the lake domain can be designated as

$$(A_1)_k \equiv \Delta Y \cdot \Delta Z_k$$

$$(A_2)_{j', k} \equiv \Delta X_{j'} \cdot \Delta Z_k$$

$$(A_3)_{j'} \equiv \Delta X_{j'} \cdot \Delta Y, \tag{39}$$

where $(A_1)_k$, $(A_2)_{j', k}$, and $(A_3)_{j'}$, denoting the cross-sectional areas normal to the equivalent x, y, and z axes, respectively, vary with the subscripted

locations.   The subvolume under computation is

$$\sigma_{j',\,k} \equiv A\,X_{j'} \cdot A\,Y \cdot A\,Z_k. \tag{40}$$

For convenience, we have denoted

$$\overline{(\ )}^{\ell}_{i',\,j',\,k'} \equiv \frac{1}{2}\,[(\ )_{\ell+1/2} + (\ )_{\ell-1/2}]_{i',\,j',\,k'} \tag{41}$$

and

$$\delta^{\ell}\,(\ )_{i',\,j',\,k'} \equiv [(\ )_{\ell+1/2} - (\ )_{\ell-1/2}]_{i',\,j',\,k'}, \tag{42}$$

where ℓ may be any of the spatial indices (i', j', k') and (i', j', k') at the integer point or at the half integer point. For example,

$$\delta^{i}\,(\overline{\psi}^{j})_{i+1/2,\,j+1/2} = \frac{1}{2}\,[\,(\psi_{i+1\ j+1} + \psi_{i+1,\,j}) - (\psi_{i,\,j+1} + Y_{i,\,j})].$$

A multiaveraging symbol as the straight forward extension of (42) is also used. For example,

$$(\overline{U}^{j\,i})_{i,\,j,\,k} = \overline{(\overline{U}^{j})}^{i}_{i,\,j,\,k} = \frac{1}{2}\,(\overline{U}^{j}_{i+1/2\ j,\,k} + \overline{U}^{j}_{i-1/2\ j,\,k}).$$

The averaging processes are performed according to the sequence of super-scripts, from the outermost inward. The outermost subscripts match with the first averaging superscript. Note also that the δ operator without a super-script, as defined in (10), implies an instantaneous convective mixing func-tion different from that defined in (41).

4.1 Finite Difference Equations

There are four prognostic variables, u', v', ψ, and T, and three diagnos-tic variables, w, p, and p', in the model. According to the adopted space-staggered grid scheme, T, ρ, and p' are computed at the integer grid points (i, j, k), u', v' at the half integer points (i + 1/2, j + 1/2, k), and w at the (i, j, k + 1/2) point. The stream function ψ is two-dimensional and is computed at the points (i, j). The basic advantage of this space-staggered arrangement of variables is to suppress the computational modes in space

17

usually introduced by the centered difference schemes. All variables are sub-
scripted according to their spatial positions (i', j', k') and are super-
scripted with the time step n, e.g., $T^n_{i,j,k}$. All transient values of a
parameter required at points other than the basic grid points during computa-
tion are usually the average of the parameter from the two immediate neigh-
boring points. For example, in computing for the **advection** of heat, the
u-component of velocity needed at point (i + 1/2, j, k) will be evaluated as

$$U_{i+1/2,\ j,\ k} = \overline{U}^{j}_{i+1/2,\ j,\ k} = \frac{1}{2}\left(U_{i+1/2,\ j-1/2,k} + U_{i+1/2,\ j+1/2,\ k}\right).$$

4.1.1 The Baroclinic Current

The finite difference equation analog to (33) for the U-component of the
shear current can be written, with respect to the **subvolumic** box centered at
(i + 1/2, j + 1/2, k), as

$$(u'\ \sigma)^{n+1} - 2a\Delta t f\ (v'\ \sigma)^{n+1} = A, \tag{43}$$

where all variables are understood as having the superscript of time step and
subscripts at the basic computational points, unless otherwise specified. The
term α is the empirically chosen stabilizing factor related to the implicit
treatment of the Coriolis term and At is the unit time step; and

$$A = (u'\ \sigma)^{n-1} + 2\Delta t\ (1 - a)\ f\ (v'\ \sigma)^{n-1} + 2\Delta t\ [P' + (F')^{n-1} + G'],$$

where the prime denotes the deviation from its vertical mean as defined before,
e.g., $P' = P - \bar{P}$. The Coriolis term is

$$f = \frac{|2\widehat{\Omega}|}{\Delta y \Delta \lambda}\ (\Delta X_j - \Delta X_{j+1}). \tag{44}$$

The baroclinic pressure gradient force is computed from density as

$$P = -\delta^i\ \overline{B}^j\ A_1, \tag{45}$$

18

where

$$
B_{i,j,k} = \begin{cases} 0, & \text{for } k = 1 \\ \sum_{k=1}^{K-1} \overline{p}^{-k} g \Delta z_{k+1/2}, & \textbf{for } k = 2, \ldots K_{ij}. \end{cases} \tag{46}
$$

The friction terms, according to (3), are

$$
F = \delta^{i}\left(\frac{\nu A_1}{\Delta x}\delta^{i} u\right) + \delta^{i}\left(\frac{\nu A_2}{\Delta y}\delta^{j} u\right) + \delta^{k}\left(\frac{\nu_1 A_3}{\Delta z}\delta^{k} u\right). \tag{47}
$$

The nonlinear terms, according to (39), are

$$
G = -\delta^{i}\left[\overline{u}^{i}\overline{\overline{(u^{j} A_1)}}^{ij}\right] - \delta^{j}\left[\overline{u}^{j}\overline{\overline{(v^{i} A_2)}}^{ji}\right]
$$

$$
+ \delta^{k}\left[\overline{u}^{k}\overline{(w^{j} A_3)}^{i}\right] - uv\,\delta^{j}(A_2). \tag{48}
$$

A prognostic equation for the v-component of the shear current with respect to point (i + 1/2, j + 1/2, k) at n time step is

$$
(v'\sigma)^{n+1} + 2a\Delta tf\,(u'\sigma)^{n+1} = A^{*}, \tag{49}
$$

where A* is similar to A as defined in (43) and P*, F*, and G* are similar to P, F, and G.

Thus the baroclinic current at all half grid points (i + 1/2, j + 1/2, k) for the advancing time step (n + 1) are

$$
(u')^{n+1} = \frac{(A + 2\alpha\Delta tfA^{*})}{\sigma\,[1 + 4(\alpha\Delta tf)^{2}]}, \tag{50}
$$

$$
(v')^{n+1} = \frac{(A - 2\alpha\Delta tA^{*})}{\sigma\,[1 + 4(\alpha\Delta tf)^{2}]}.
$$

Notice that the basic time differencing in the model is the leap-frog scheme. It may cause the temporal "splitting" phenomena in the solution in a long-term integration (Lilly, 1965). Therefore, the Euler-Matsuno (implicit

19

backward) scheme is applied periodically in order to suppress the high frequency computational noise that results from the exclusive use of the centered time differencing scheme. In that case, instead of (43), (49), and (50) for the velocity, the shear current is obtained in two steps, one forward and one backward step by solving

$$q_*^{n+1} - q^n = \Delta t \{P^n + F^n + G^n + f [\alpha q_*^{n+1} + (1 - \alpha) q^n]\}$$

$$\tag{51}$$

$$q^{n+1} - q^n = \Delta t \{P_*^n + F_*^{n+1} + G_*^{n+1} + f [\alpha q^{n+1} + (1 - a) q^n]\},$$

where q is either u' or v' and the subscript * indicates the intermediate advanced quantity.

4.1.2 The Vorticity Equation

The finite difference vorticity equation according to (31) is computed with respect to (i, j) points,

$$\nabla^2 \frac{\psi_t}{D} = \delta^i \left\{ \overline{\left[\frac{f}{D} \delta^j (\overline{\psi}^i) \right]}^j \right\} - \delta^j \left\{ \overline{\left[\frac{f}{D} \delta^i (\overline{\psi}^j) \right]}^i \right\}$$

$$- \frac{1}{\rho_o} \delta^i \left\{ \overline{\left[\frac{g}{D} \sum_{k=1}^{K} (\sum_{k'=1}^{k} \delta^j (\overline{\rho}^i)_{k'+1/2} \Delta Z_{k'+1/2}) \Delta Z_k \right]}^j \right\}$$

$$+ \frac{1}{\rho_o} \delta^i \left\{ \overline{\left[\frac{g}{D} \sum_{k=1}^{K} (\sum_{k'=1}^{k} \delta^i (\overline{\rho}^j)_{k'+1/2} \Delta Z_{k'+1/2}) \Delta Z_k \right]}^i \right\}$$

$$+ \frac{1}{\Delta X} \delta^i \left\{ \overline{\left[\frac{1}{D} \sum_{k=1}^{K} (G* + F*) c \right]}^j \right\}$$

$$- \frac{1}{\Delta y} \delta^j \left\{ \overline{\left[\frac{1}{D} \sum_{k=1}^{K} (G + F) \sigma \right]}^i \right\} \tag{52}$$

and

$$\nabla^2 \frac{\psi}{D} = \delta^i \left\{ \frac{\Delta Y}{\Delta X} \overline{\left[\frac{1}{D} \delta^i (\overline{\psi})^j \right]}^j \right\}$$

$$+ \delta^j \left\{ \frac{\Delta X}{\Delta Y} \overline{\left[\frac{1}{D} \delta^j \overline{(\psi)^i} \right]}^i \right\} \tag{53}$$

Note that (53) is a nine-point finite difference form of the Laplacian operator with a bathymetry of the lake incorporated. It can be approximated to a slant five-point scheme if AX = AY. However, the slant five-point scheme may

cause computational noise in the checkboard pattern, especially with irregular boundaries and with the irregular external forcing (Takano, 1973, personal communication). We have modified the regular five-point scheme with the four-point mean bottom effect incorporated in it as

$$\nabla^2 \left(\frac{\psi}{D}\right)_{i,\,j} = \left(\frac{\psi}{\bar{D}}\right)_{i,j+1} + \left(\frac{\psi}{\bar{D}}\right)_{i+1,\,j} + \left(\frac{\psi}{\bar{D}}\right)_{i,\,j-1}$$

$$+ \left(\frac{\psi}{\bar{D}}\right)_{i-1,\,j} - 4\left(\frac{\psi}{\bar{D}_0}\right)_{i,j}, \tag{54}$$

where $\bar{D}$ is the average depth at the grid point taken from the four neighboring velocity points. The three mentioned schemes were tested in the Lake Ontario model and they showed essentially the same results. Therefore, we have adopted (54) for the lake model. Since the computational points of the stream function coincide with the coastal points along the lake, (54) is solved by accelerated relaxation with the stream function specified on all lateral boundary points. Since the momentum advections and the bottom topography are included in the model, there exists energy transformation between the barotropic and the baroclinic modes. It is convenient to have the stream function advanced with the same time step as the shear current in the model.

4.1.3 The Barotropic Current

The barotropic velocity components at the half-grid points, $(i + 1/2, j + 1/2)$ are

$$u = -\frac{1}{D\Delta y}\,\delta^j\,\bar{\psi}^{\,i} \quad \text{and}$$

$$v = \frac{1}{D\Delta X}\,\delta^i\,\bar{\psi}^{\,j}. \tag{55}$$

4.1.4 The Vertical Velocity

From the continuity equation, the vertical velocity can be obtained at the $(i, j, k + 1/2)$ points as

$$w = w_{k-1/2} - \frac{\Delta Z_k}{\sigma k}\,[(A_1)_k\,\delta^i\,(\bar{u}^{\,j})_k + \delta^j\,(A_2\,\bar{v}^{\,i})_k], \tag{56}$$

with $w_{i,\,j,\,1/2} = 0$ at the surface. The vertical velocity at the velocity point $\bar{w}_{i+1/2,\,j+1/2,\,k+1/2}$ is consistently the averaging value of the vertical velocities of the four neighboring points.

It is readily shown that the total kinetic energy is balanced for the whole lake for the above finite differencing scheme. There is no source or sink of kinetic energy other than the viscous effect in the system, except a small portion of energy transformation from kinetic energy to potential energy that is also in balance with the reverse transformation, i.e., from the potential energy to the kinetic energy.

4.1.5 Temperature Equation

The temperature is calculated at all whole grid points (i, j, k). The finite difference form of (8) is

$$(T\sigma)^{n+1} = (T\sigma)^{n-1} + 2\Delta t \, (H^n + Q^{n-1}),$$

(57)

where

$$H = - [A_1 \, \delta^i \, (\overline{T}^i \overline{u}^j)] + \delta^j \, [A2 \, (\overline{T}^j \overline{v}^i)] + A_3 \, \delta^k \, (\overline{T}^k w)$$

(58)

and

$$Q = \frac{\kappa A_1}{\Delta X} \, \delta^i \, (\delta^i T) + \frac{1}{\Delta Y} \, \delta^i \, (\kappa \, A_2 \, \delta^j T) - A_3 \, \delta^k \, \left(\frac{\kappa_1}{\Delta Z} \, \delta^k T \right).$$

(59)

Later, it will become clear that the only source and sink for the potential energy in the lake domain, besides the small portion internally transformed from the kinetic energy, are the heat fluxes through the surface and the diffusive dissipations.

4.2 Finite Difference Boundary Conditions

All the mesh grid points on the solid lateral boundaries coincide with the calculating points of $\psi_{i, j}$ and $T_{i, j, k}$. Understanding that the other two dummy indices are not specified, the zero flux condition at all solid boundaries leads to

$$T_{\ell*+1} = T_{\ell*-1},$$

(60)

where $\ell*$ is the index normal to the boundary at the boundary such as i*, I and j*, J.

$$\psi_{i, j} = \text{Constant}$$

(61)

at all lateral boundaries.

22

Since $V_{i+1/2, j+1/2, k}$ is calculated at one-half grid distance inside the boundaries, the no-slip condition leads to

$$V_{\ell*-1/2} = -V_{\ell*+1/2}.$$ (62)

The vertical velocities are

$$w_{i, j, 1/2} = 0 \quad \text{at} \quad z = 0,$$ (63)

and

$$W_{i, j, K+1/2} = -\frac{\overline{u}^j}{\Delta X} \delta^i \overline{D}^j - \frac{\overline{v}^i}{\Delta Y} \delta \overline{D}^i \quad \text{at} \quad Z = -D.$$ (64)

The bottom stress is parameterized as

$$\frac{\nu_1}{\Delta Z_{K+1/2}} \delta^k V_{i+1/2, j+1/2, K+1/2} = \left(\frac{\tau_b}{\rho_o}\right)_{i+1/2, j+1/2}, \quad z = -D,$$ (65)

where τ_b is computed according to (13).

The upper boundary conditions are

$$\frac{\kappa_1}{\Delta Z_{1/2}} \delta^k T_{i, j, 1/2} = \frac{Q_s}{\rho_o C_p}$$ (66)

$$\frac{\nu_1}{\Delta Z_{1/2}} \delta^k V_{i+1/2, j+1/2, 1/2} = \frac{\tau_s}{\rho_o} \quad \text{at} \quad z = 0,$$ (67)

where Q_s and τ_s are computed from (14) and (21), respectively.

4.3 Special Treatment of Irregular Boundaries

According to the space-staggered scheme in the model, the locations of prognostic variables T and ψ and diagnostic variables ρ, p, and w coincide with the coastal boundaries, where at least one of the four neighboring points $(i \pm 1/2, j \pm 1/2)$ is out of the domain of interest. The use of a centered difference at these boundary points is not practical because velocities are undefined on land. With the boundary conditions previously specified, it is necessary that all terms in the heat and continuity equations are properly weighted by their corresponding volumes at these corner points for consistency and for conservation of desired properties when the computation is carried out on a boundary.

23

In the lake-scale model, all indices of irregular boundaries are different from those on the land as well as in the lake as summarized in Figure 3. The
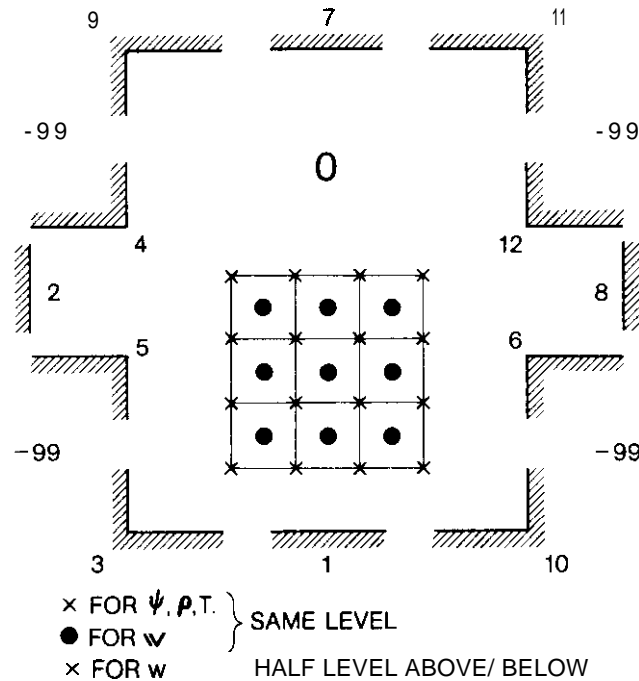
Summary of Indexes and locations of Variables

× FOR ψ, ρ,T. } SAME LEVEL
● FOR v }
× FOR w HALF LEVEL ABOVE/ BELOW

Figure 3. Summary of indexes and relative locations **of** *prognostic variables.*

interior points in the lake are indexed as 0 and all land points are indexed as a negative integer number, while all boundary points are indexed as a posi- tive integer number from 1 to 12 to indicate all possible irregular cases in the lake. Since the velocity at the half grid points $(i + 1/2, j + 1/2)$ bears the same index as the lower-left corner whole grid point (i, j), all velocity indices smaller than or equal to 6 are in the lake, while indices greater than 6 are boundary points on the land. Since the numerical schemes in the model are constructed in the flux form, the volume of the computational box is closely related to the flux quantity of heat or momentum in the calculation. Three examples are given below to illustrate the specially weighted treatment for the irregular corner points.

The flux forms of the advection and the diffusion of heat on a straight boundary, e.g., the index 1 of a southern boundary, are

$$\nabla \cdot (VT)_{i, 1, k} \quad \sigma'_{1, k} = (u_{i+1/2, 3/2, k} \overline{T}^i_{i+1/2, 1, k}$$

$$- u_{i-1/2, \; 3/2, \; k} \; \overline{T}^i_{i-1/2, \; 1, \; k}) \; \dfrac{(A_1)_k}{2}$$

$$+ (\overline{v}^1_{i, \; 3/2, \; k} \; \overline{T}^j_{i, \; 3/2, \; k}) \; (A_2)_{3/2, \; k} \tag{68a}$$

and

$$(\kappa \nabla^2 T)_{i, \; 1, \; k} \; \sigma'_{1, \; k} = \left[\left(\kappa \dfrac{\delta T}{\delta X} \right)_{i+1/2, \; 1, \; k} \right.$$

$$\left. - \left(\kappa \dfrac{\delta T}{\delta x} \right)_{i-1/2, \; 1, \; k} \right] \dfrac{1}{2} (A_1)_k + \left(\kappa \dfrac{\delta T}{\delta Y} \right)_{i, \; 3/2, \; k} (A_2)_{3/2, \; k}$$

$$= \dfrac{\kappa (A_1)_k}{2 \Delta X_1} \delta^i (\delta^i T)_{i, \; 1 \; k} + \dfrac{\kappa (A_2)_{3/2, \; k}}{AY} \delta^j T_{i, \; 3/2, \; k'} \tag{69a}$$

where A_1, A_2 are defined in (39) and σ' is the effective computational sub-volume similar to (40). Notice that in (68a) and (69a), both the velocity and the temperature boundary conditions (60) and (62) have been applied. The term σ' is essentially weighted by half as much as that of the subvolume away from the southern boundary in the interior of the lake.

For an indented corner point such as the index 3 corner boundary, only one velocity with respect to the computing point is available in the lake. The advection and diffusion terms in the heat energy equation become, for example, at point (1, 1, k),

$$V \cdot (\nabla T)_{1, \; 1, \; k} \; \sigma'_{1, \; k} = (u_{3/2, \; 3/2, \; k} \; \overline{T}^i_{3/2, \; 1, \; k}) \; (A_1)_k$$

$$+ (v_{3/2, \; 3/2, \; k} \; \overline{T}^j_{1, \; 3/2, \; k}) \; (A_2)_{3/2, \; k'} \tag{68b}$$

where σ' is weighted by 1/4 as much as that of a regular subvolume, and

$$(\kappa \nabla^2 T)_{1, \; 1, \; k} \cdot \sigma'_{1, \; k} = \dfrac{\kappa (A_1)_k}{2 \Delta X_1} \delta^i T_{3/2, \; 1, \; k}$$

$$+ \dfrac{\kappa (A_2)_{3/2, \; k}}{2 AY} \delta^j T_{3/2, \; 1, \; k} \cdot \tag{69b}$$

At a protruding corner, such as the point of index 4, the advection and the diffusion terms are

$$\nabla \cdot (\nabla T)_{i, \; j, \; k} \; \sigma'_{j, \; k} = \overline{u}^j_{i+1/2, \; j, \; k} \; (A_1)_k - u_{i-1/2, \; j-1/2, \; k} \; \dfrac{(A_1)_k}{2}$$

25

$$+ v_{i+1/2,\ j+1/2,\ k} \quad \frac{(A_2)_{j+1/2,\ k}}{2} - "_{i,\ j-1/2,\ k}\ (A_2)_{j-1/2,\ k}\cdot \qquad (68c)$$

where σ' is weighted by 3/4 as much as that of a regular subvolume and

$$(\kappa\nabla^2 T)_{i,\ j,\ k}\ \sigma'_{j,\ k} = \frac{\kappa(A_1)_k}{\Delta X_j}\ \delta^i T_{i+1/2,\ j,\ k} - \frac{\kappa(A_1)_k}{2AX_j}\ \delta^i T_{i-1/2,\ j,\ k}$$

$$+ \frac{\kappa(A_2)_{j+1/2,\ k}}{2\Delta Y}\ \delta^j T_{i,\ j+1/2,\ k} - \frac{\kappa(A_2)_{j-1/2,\ k}}{\delta Y}\ \delta^j T_{i,\ j-1/2,\ k}\cdot \qquad (69c)$$

All other boundary points are treated in a similar manner to those shown in (68) and (69).

4.4 Hydrostatic Stability

At places where excessive upward heat flux occurs and where evaporation exceeds precipitation by a large amount, a layer of heavy cold water will be formed in the upper layers of the lake. Whenever the local lapse rate of density is less than the vertical lapse rate, thus ensuring a marginally stable vertical density distribution, hydrostatic instability exists in the adjacent layers. Since instability in the real lake usually lasts for a short period of time, an instantaneous convective adjustment mechanism is used in the model. **Let**

$$\gamma_\rho = - \left(\frac{\rho_{k-1} - \rho_k}{\Delta Z_{k-1/2}} \right)$$

be the equivalent lapse rate of density between layers. A small positive value, ε_ρ, is assumed since there may exist a slight inversion in density within the marginal stability limit. In the model, the lapse rate between layers is computed and compared with ε_ρ. If

$$-\gamma_\rho < \varepsilon_\rho \quad \text{is stable,}$$

$$\qquad (70)$$

then $\qquad -\gamma_\rho > \varepsilon_\rho \quad \text{is unstable,}$

where ε_ρ is estimated from the average density distribution in the lake. The **marginal** stability criteria for temperature is estimated from ε_ρ and the coefficients for temperature expansions in the mean state of the lake. Then, in case instability is detected between layers $k - 1$ and k, the temperatures

26

In these vertical layers are mixed into quasi-homogeneity

$$T_k^* = \frac{T_k \Delta Z_k + (T_{k-1} - \varepsilon_T \Delta Z_{k-1/2}) \; \Delta Z_{k-1}}{\Delta Z_{k-1} + \Delta Z_k}$$

$$T_{k-1}^* = T_k^* + \varepsilon_T \Delta Z_{k-1/2}, \tag{71}$$

where the superscript * indicates the adjusted value after mixing and ε_T is the marginal stable criterion for temperature distributions. These stability criteria and the adjusting processes are applied to all layers in the column, and the procedure is repeated whenever there is more than one unstable sub-column until stability has been reached for the whole column.

4.5 Energy Conservation

In the construction of the numerical scheme using the box method, great emphasis has been given to the conservation of energy. It is vitally neces-sary that the total integral of energy for the whole basin is consistent and in balance. It is readily shown that there are no energy sources or sinks within the whole thermo-hydrodynamic system of the model lake other than the frictional and diffusive terms. Considering the mean state of the lake with constant energy input (i.e., wind stress, net heat fluxes) to be used to overcome the dissipation effects, the sum of kinetic and potential energy in the whole system should be conserved when the model lake approaches the quasi-equilibrium state.

Let <K> be the overall kinetic energy:

$$<K> = I, \; \frac{1}{2} \rho_o V^2 dV. \tag{72}$$

Equation (29) leads to the separation of the total kinetic energy into two parts: one for the vertical mean current, i.e., the barotropic mode,

$$<K> = \int_A \frac{D}{2} \rho_o V^2 dA \tag{73}$$

and the other for the vertical shear current, i.e., the baroclinic mode,

$$<K'> = \int_V \frac{1}{2} \rho_o V'^2 dV. \tag{74}$$

27

The finite difference form of (72) is

$$\langle K \rangle = \sum_{k=1}^{K} \sum_{j=j*}^{J-1} \sum_{i=i*}^{I-1} (\hat{K} + K').$$ (75)

Then the time rate of change of $\langle K \rangle$ is

$$\langle K_t \rangle = \langle K_t + K'_t \rangle,$$ (76)

where

$$(K)_t = \rho_o \hat{V} \cdot \hat{V}_t$$ (77)

$$(K')_t = \rho_o V' \cdot V'_t.$$ (78)

The time rate of change of the kinetic energy of the baroclinic mode can be obtained from the dot product of (50) and $\rho_o V'$ before the time advancement. That is, with reference to the (i + 1/2, j + 1/2, k) points, unless otherwise specified,

$$\langle K'_t \cdot \sigma \rangle = \langle \rho_o A' \cdot V' \rangle = \rho_o \langle I_1 + I_2 + I_3 + I_4 \rangle,$$ (79)

where the two components of A are as shown in (43) and (49) except for the time step, i.e.,

$$A = P^n + F^{n-1} + G^n + (2\Omega \times V \cdot \sigma)^n,$$ (80)

where

$$I_1 = [P'u' + P*'v'],$$ (81)

$$I_2 = [F'u' + F*'v'],$$ (82)

$$I_3 = [G'u + G*'v'],$$ (83)

28

$$I_4 = [fv'\sigma u' - fu'\sigma v'], \tag{84}$$

where P, F, and G and P*, F*, and G* are defined in (45), (47), (48), and their similar equations. The time rate of change of the barotropic kinetic energy can be written, with respect to points $(i + 1/2, j + 1/2)$, as

$$\langle \rho_o \, \sigma \, \hat{V} \cdot \hat{V}_t \rangle = \rho_o \sum_{j=j*}^{J-1} \sum_{i=i*}^{I-1} \left[\frac{\Delta x}{\Delta y D} \cdot \delta^j \overline{(\psi)}^i \cdot \delta^j \overline{(\psi_t)}^i \right.$$
$$\left. + \frac{\Delta y}{\Delta x_j D} \cdot \delta^i \overline{(\psi)}^j \cdot \delta^i \overline{(\psi_t)}^j \right], \tag{85}$$

which can be written, with respect to the same indices, as

$$\langle K_t \cdot \sigma \rangle = \rho_o \sum_{j=j*}^{J-1} \sum_{i=i*}^{I-1} \left\{ \delta^j \left[\frac{\Delta x}{D\Delta y} \overline{\psi}^i \overline{(\delta^j \overline{\psi}_t^i)}^j \right] \right.$$

$$- \frac{\Delta x}{\Delta y} \overline{\left[\overline{\psi}^i \, \delta^j \frac{(\delta^j \overline{\psi}_t^i)}{D} \right]}^j + \delta^i \left[\frac{\Delta y}{D\Delta x} \overline{\psi}^j \cdot \delta^i \overline{(\psi_t)}^j \right]$$

$$\left. - \frac{\Delta y}{\Delta x} \overline{\left[\overline{\psi}^j \, \delta^i \frac{(\delta^i \overline{\psi}_t^j)}{D} \right]}^i \right\}. \tag{86}$$

The flux terms vanish after summing over the whole domain because $\psi_{ij} = 0$ on all lateral boundaries. The zero stream function along all boundaries also permits index shifting in summation. This then easily leads to

$$\langle K_t \cdot \sigma \rangle = \rho_o \sum_{j=j*+1}^{J-1} \sum_{i=i*+1}^{I-1} \psi_{i,j} \left(\nabla^2 \frac{\psi_t}{D} \right)_{i,j}, \tag{87}$$

where $\nabla^2 \dfrac{\psi_t}{D}$ is defined in (52). The vertical mean kinetic energy becomes

$$\langle K_t \cdot \sigma \rangle = - \rho_o \sum_{j=j*+1}^{J-1} \sum_{i=i*+1}^{I-1} (I_5 + I_6 + I_7)_{i,j}, \tag{88}$$

where, with indices at (i, j) points,

$$I_5 = \psi \left[\frac{\delta^i \overline{\frac{\hat{G}^*}{D}}^j}{\Delta X} - \frac{\delta^j \overline{\frac{\hat{G}}{D}}^i}{\Delta Y} \right], \tag{89}$$

29

$$I_6 = \psi \left[\frac{\delta^i \; \overline{\dfrac{\hat{F^*}}{D}}^j}{\Delta X} - \frac{\delta^j \; \overline{\dfrac{\hat{F}}{D}}^i}{AY} \right], \tag{90}$$

$$I_7 = \psi \; [\delta^j f \; \delta^i \overline{\psi}^i]. \tag{91}$$

The total time rate of change of kinetic energy for the whole ocean is

$$\langle K_t \; \sigma \rangle = \sum_{j=j^*}^{J-1} \; \sum_{i=i^*}^{I-1} \; \sum_{k=1}^{K} \; \rho_o \; (I_1 + I_2 + I_3 + I_4)$$

$$+ \sum_{j=j^*+1} \; \sum_{i=i^*+1} \; (I_5 + I_6 + I_7). \tag{92}$$

It is easy to show that the work done by the pressure gradient force increases the kinetic energy at a rate equal to the rate of decrease in potential energy,

$$\langle \rho_o \; I_1 \rangle = \sum_{j=j^*}^{J-1} \; \sum_{i=i^*}^{I-1} \; \sum_{k=2}^{K} \; [-g \; (\rho w)_{k+1/2} \; \sigma_{j, \; k}]. \tag{93}$$

The nonlinear terms do no net work:

$$\langle I_3 \rangle + \langle I_5 \rangle = 0. \tag{94}$$

The Coriolis term does no net work:

$$\langle I_4 \rangle + \langle I_7 \rangle = 0. \tag{95}$$

The only sources and sinks for momentum in the whole hydrodynamic system are in the viscous terms $[I_2]$ and $[I_6]$.

The total available potential energy with reference to the bottom is

$$\langle \phi_{i, \; j, \; k} \; \sigma_{j, \; k} \rangle = \langle g \; \rho_{i, \; j, \; k} \; (D_{i, \; j} + z)_k \; \sigma_{j, \; k} \rangle. \tag{96}$$

The time rate of change of the potential energy is totally dependent on the time rate of change of the density, which is a function of temperature. It is clear that the vertical advection term, $(\rho w)_z$ has produced an increase in potential energy exactly balancing the rate of decrease in potential energy due to the pressure gradient force. The only thermal sources and sinks in the whole system are in the diffusive terms. Therefore, the total potential

and kinetic energy in the model is conserved and all the required integral
constraints are satisfied under the equilibrium state, i.e., the mechanical
energy input as the boundary condition is balanced by the frictional dissipa-
tions and the heating effect is balanced by the thermal diffusions.

5. PRELIMINARY RESULTS

In a preliminary study on Lake Ontario, we used a 0.05" grid in the off-
shore direction and a 0.1" grid in the longshore direction for the horizontal
separations (about 8 km in the east-west and 5 km in the north-south direction)
and chose four variable vertical layers of thickness 20 m, 30 m, 60 m, and 90
m with a total maximum depth of 200 m.   The lateral configuration and bottom
topography of Lake Ontario were used as the reference lake.   In the computa-
tion, since the trapezoidal implicit scheme employed for treating the Coriolis
effect is unconditionally stable, the maximum time step is governed essentially
by the leap-frog scheme.   Based on the internal gravity wave, the Courant-
Fredericks-Lewy condition is satisfied in the present coarse grid model by
taking a time step of 1.5 hr.   All constants used in the model are summarized
in Table 1.   The computation sequence is that first the velocity field is cal-
culated and then the temperature; hence the density is obtained at any time
step.

Taking the future commitment to study other lakes into consideration, we
programmed the lake model in such a flexible manner that it could be used for
simulations of any lake at any location with only a minor change in the dimen-
sional and mesh indexes.   With the possible limitations of the central core
memory of the available computer in mind, the computations of the lake domain
were carried out in a sequence of blocks.   Each block contains a minimum of
three strings of j values independent of k (layer); this is necessary to per-
form one latitudinal computation in the central core memory. According to
the climatology of the Great Lakes, the winds encountered in Lake Ontario tend
to parallel the northeast-southwest axis of the St. Lawrence River (Department
of commerce, 1959), similar to the longshore axis of the lake.   IFYGL data
also confirmed that the prevailing mean winds during the field seasons were
generally from the southwest, except during spring and the month of November,
when they were from the northeast (see,e.g.,*IFYGL Bulletin* 15).   We have
carried out two demonstration runs with a wind stress of 0.5 dyne/cm^2, which
is equivalent to wind about 5 m/s from the southwest and the northeast,
respectively.   The southwest wind is comparable to July 1972 conditions and
the northeast wind to November 1972 conditions.

Figure 4 shows the vertically integrated stream function after lo-days
integration of the model in Lake Ontario under a uniform wind from the south-
west and with surface heating similar to the July atmosphere.   Since the
forcing functions, namely wind stress and heating, do not vary with time, we
are studying the situation analogous to the steady monthly mean state in the
lake.   Under the assumption that the July wind has a resultant equivalent to
about 500 cm/s from the southwest, the mass transport forms a two-gyre mean
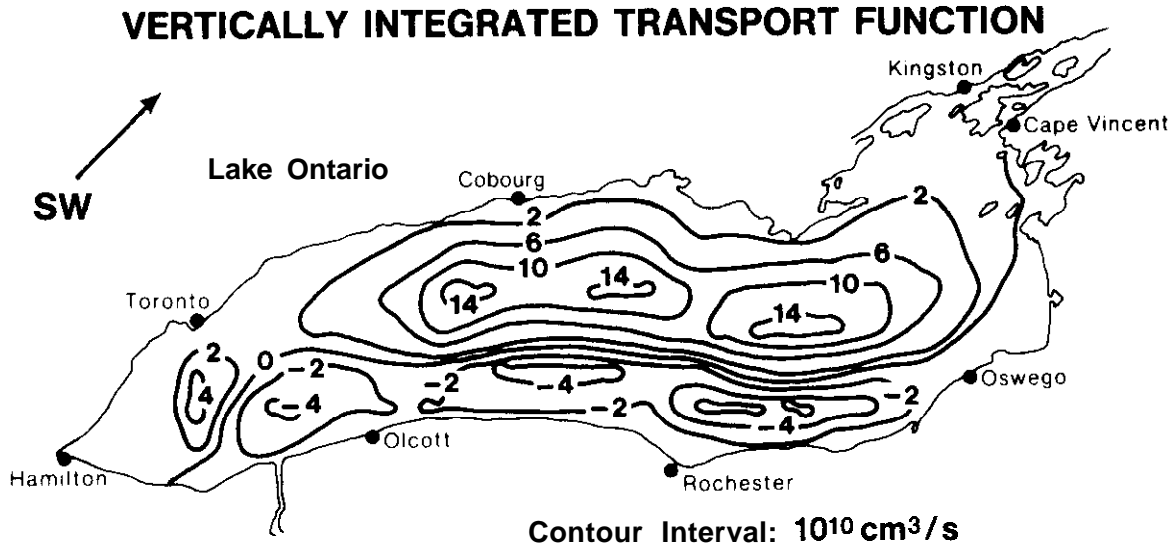circulation pattern, an elongated, anticyclonic gyre in the north and a

31

VERTICALLY INTEGRATED TRANSPORT FUNCTION

Figure 4. *Vertically integrated transport function under the southwesterly wind.*

cyclonic gyre in the south with a nodal line slightly south in the middle. The stream function indicates that the mass flow is mostly eastward, in the direction of the wind, near both the north and the south shore regions and is westward, against the wind, in the middle of the lake. A similar flow pattern has been produced for similar wind conditions in Lake Ontario by others, notably Rao and Murty (1970). Note that the vertically integrated stream function is considered to be the simulated transport state after 10 days of steady wind. Figure 5 shows the time evolution of the total kinetic energy, the vertical mean kinetic energy, and the kinetic energy due to the shear current in the Lake Ontario model. In the spin-up stage, the dominant feature is the inertial oscillation at a period of 17.5 hrs as vividly indicated in Figure 5. Figure 5b shows the increasing kinetic energy of the barotropic current caused mostly by the external forcing, of which the surface wind is the dominant component. The barotropic kinetic energy reaches a quasi-steady state rather fast (after 2-3 days), while the baroclinic kinetic energy (Figure 5c) and the total kinetic energy (Figure 5a) continue to oscillate around an asymptotic state. The variations of all three curves in Figure 5 are very small after lo-days integration. It is assumed that the barotropic response in the lake as shown in Figure 5 by the stream function has reached a steady state after 10 days. However, there exists a long-term tendency toward slightly decreasing energy in the barotropic mode and in the total energy as well as slightly increasing energy in the baroclinic mode as indicated in Figure 5. The baroclinic influences due to thermal effects are still progressing after 10 days as the baroclinic currents are still increasing. The aforementioned weak energy transformation between the barotropic mode and the baroclinic mode, as indicated in the tendencies of the two energy curves,
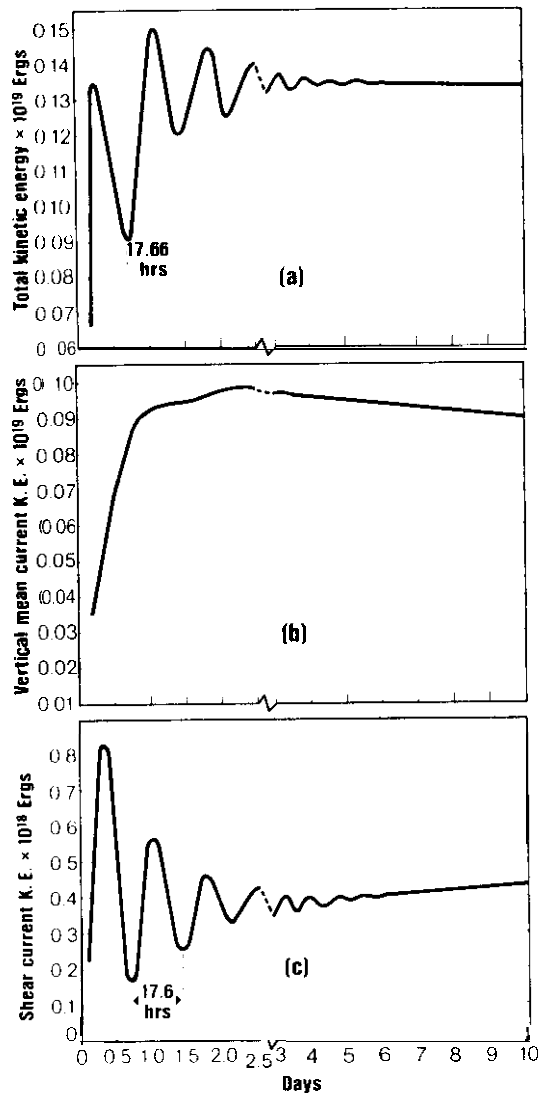
32

Figure 5. Time **evolution of** the kinetic energy (K. E.) in the Lake Ontario model
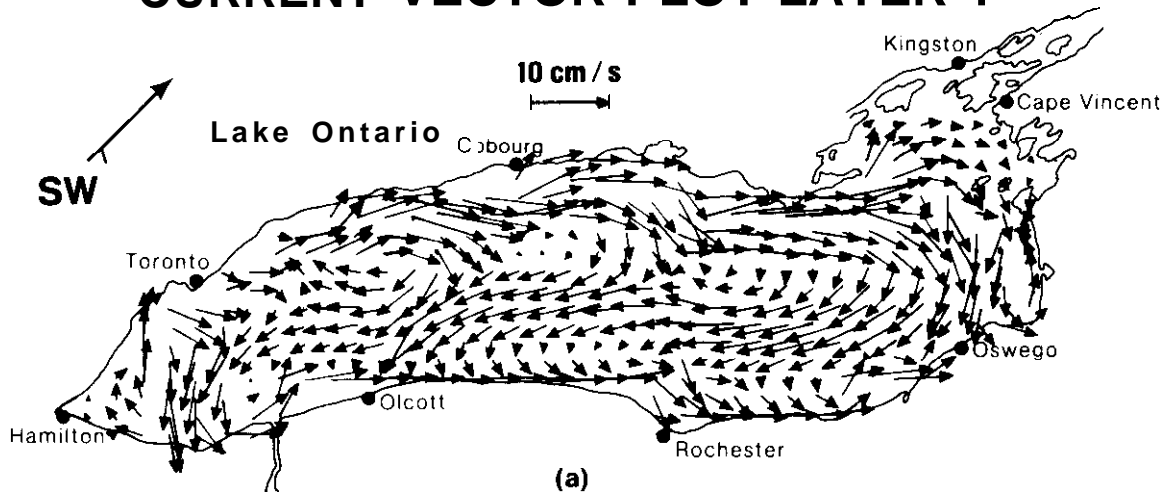
(a) Total kinetic energy

(b) Kinetic energy **of** the barotropic current

(c) Kinetic energy of the baroclinic current.

are due to the incorporation of the nonlinear effect of advection and the bottom topographic torque in the model.

33

Figure 6 shows the current vector plot of the surface layer at 10 m below the surface and of the second layer at 35 m below the interface. Figure 6a shows generally that surface currents at both the northern and the southern coastal boundaries flow with the wind and that there is a return flow against the wind in the middle of the lake. The coastal jet phenomenon is clearly

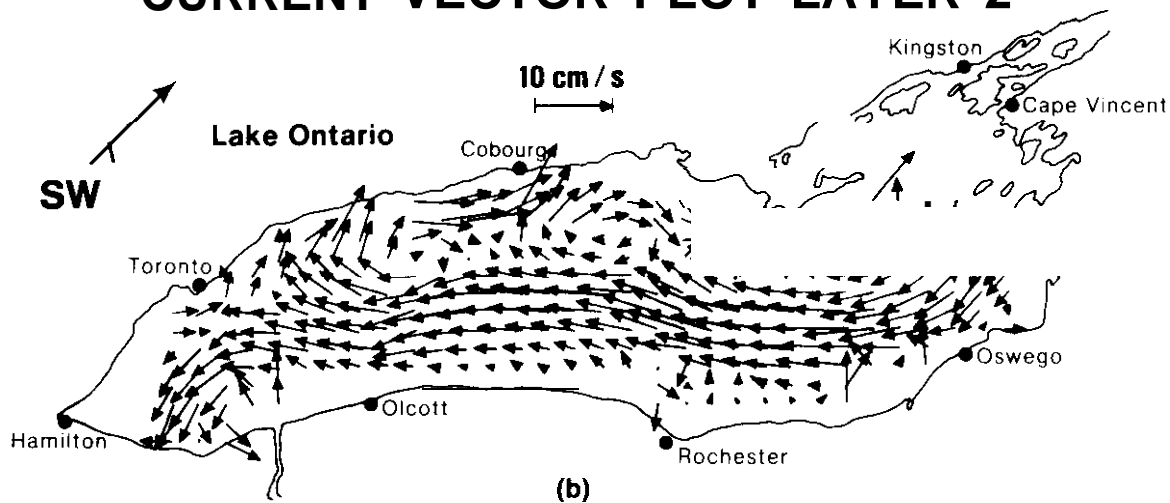## CURRENT VECTOR PLOT LAYER 1

(a)

CURRENT VECTOR PLOT LAYER 2

(b)

Figure 6. Layered current vector plots under the southwesterly wind

(a) at 10 m depth

(b) at 30 m depth.

34

demonstrated. The maximum coastal current is about 10 cm/s. Between the coastal jets and the returning flow are the Ekman currents, flowing at an angle away from the wind. The current pattern indicates that surface currents in the shallow coastal regions respond to the wind quickly and completely, and that a return flow is formed along the deep bathymetry in the middle lake to balance the surface pressure build-up at the downwind end of the lake. Figure 6b shows that the current at a depth of 35 m is dominated by the return flow caused by the surface tilt due to wind set-up. In the deep layers, currents are weak, thus balancing flow in the direction opposite to the wind. Figure 7 shows three cross-sectional plots of the east-west component of current.
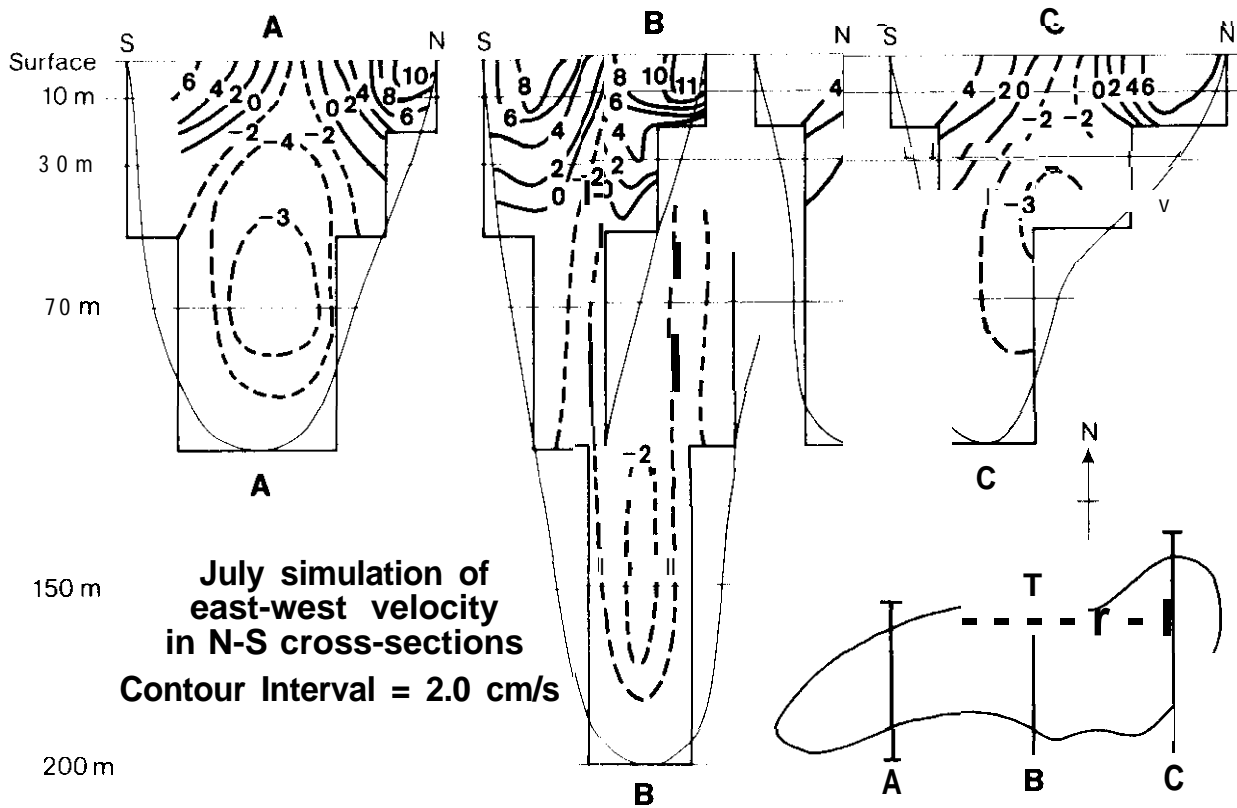

July simulation of east-west velocity in N-S cross-sections

Contour Interval = 2.0 cm/s

Figure 7. North-south cross-sectional plots 0 f the east-west component 0 f velocity under the southwesterly wind.

It further clearly portrays the strong coastal jets near the boundaries and the weak, broad return flow in the middle of the lake. The general circulation current agrees satisfactorily with other similar studies (c.f., Simons, 1975; Baba, 1974). However, it does not compare well with July 1972 IFYGL data (Pickett and Richards, 1975). The current meter data at 15 m (or 16 m) coincide well with the simulated currents in the southern half and the eastern portion of the lake. The model current near the north shore flows in the opposite direction to that of the observations. Figure 8 shows the vertical

VERTICAL VELOCITY at 10 m
(FOR WARMING UP SIMULATION)

↑↑↑ = 1.0 – 5.0 m/day
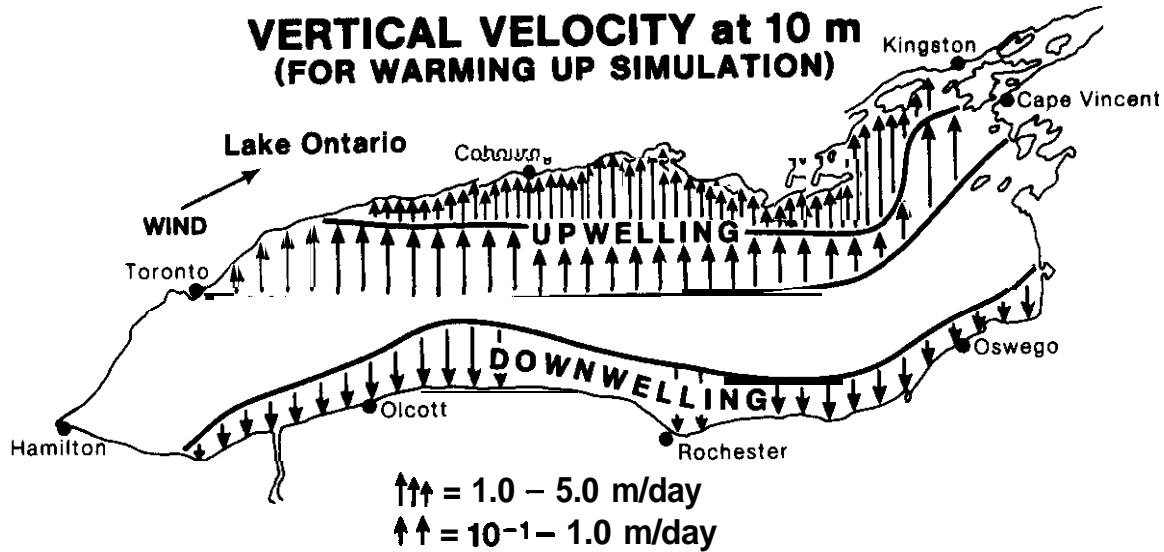↑ ↑ = 10⁻¹ – 1.0 m/day

Figure 8. Vertical velocity under the southwesterly wind.

current contour plot after 10 days. It shows a strong upwelling along most of the northern boundary and downwelling along most of the southern boundary. Figure 9 shows three cross-sectional temperature plots in the lake. Though the temperature distribution was not yet steady at the time these data were collected, the tilting of isotherms toward the north is clearly demonstrated. The discrepancy between the model and the observational data near the northern boundary might be the result of upwelling along the north shore. The upwelling pushes the thermocline up in the northern part of the lake. It may serve as a separation layer for the surface flow, which is based on Ekman dynamics, and the return flow, which is opposite in direction to the surface flow and is dominated by the pressure gradient. Detailed verification of the model is beyond the scope of this report.

When the wind is blowing from the northeast, the vertically integrated mass transport has the same pattern as that of the southwesterly wind except that the flow directions are totally reversed (Figure 10). There is still the two-gyre circulation pattern, the larger elongated cyclonic gyre in the north and the smaller elongated anticyclonic gyre in the south. The major flow is still along the deep bathymetry of the lake toward the east. Figure 11 shows the layer current vector plots for the first two layers at 10 m and
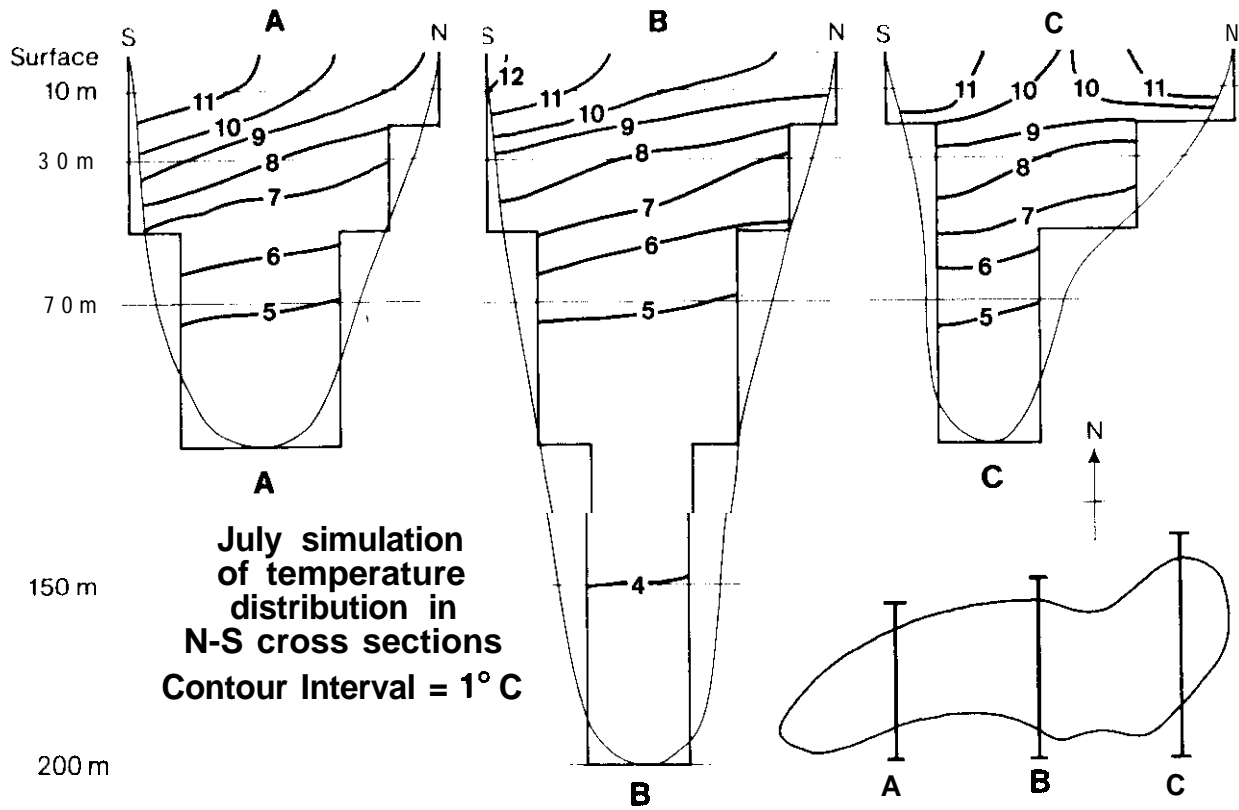
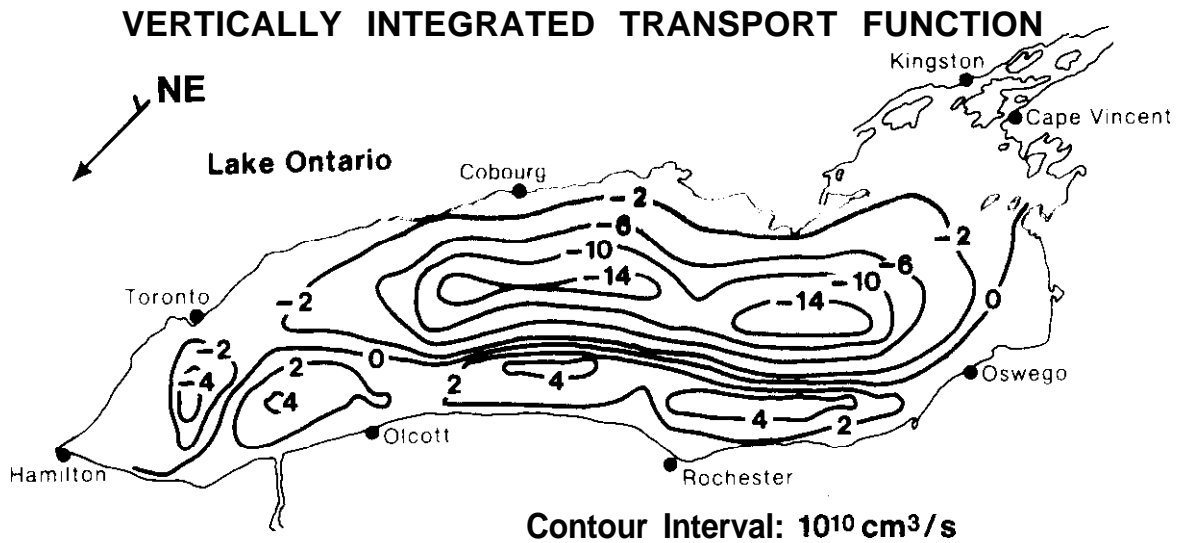*Figure 9. North-south cross-sectional plots of temperature under the southwesterly wind.*
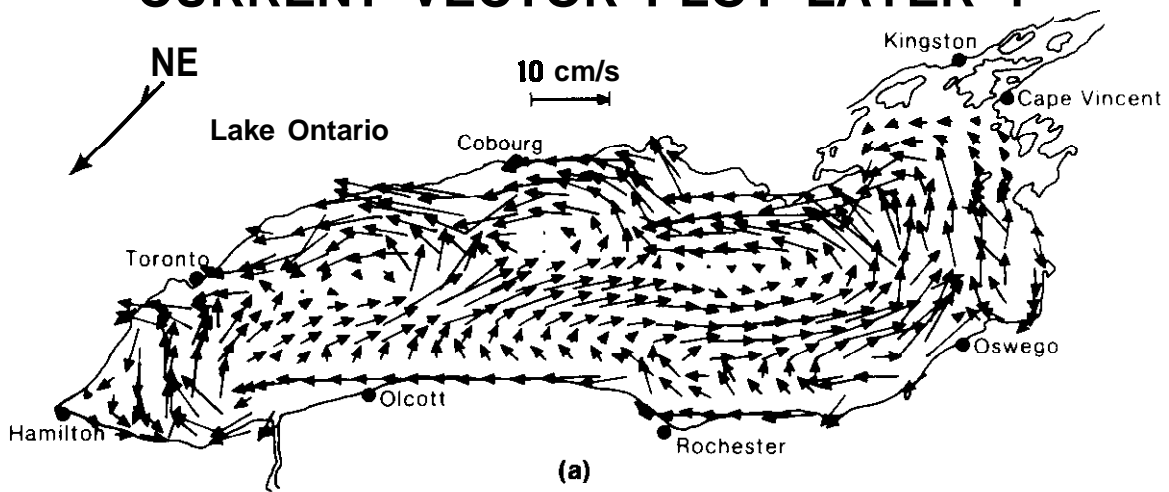

Figure 10. Vertically integrated transport function under the north-easterly wind.

37

CURRENT VECTOR PLOT LAYER 1

(a)

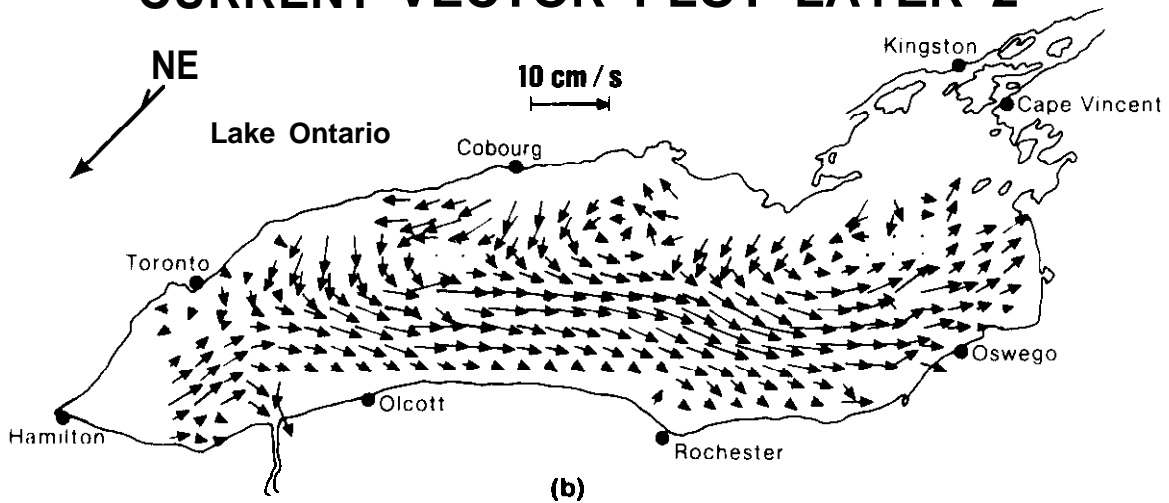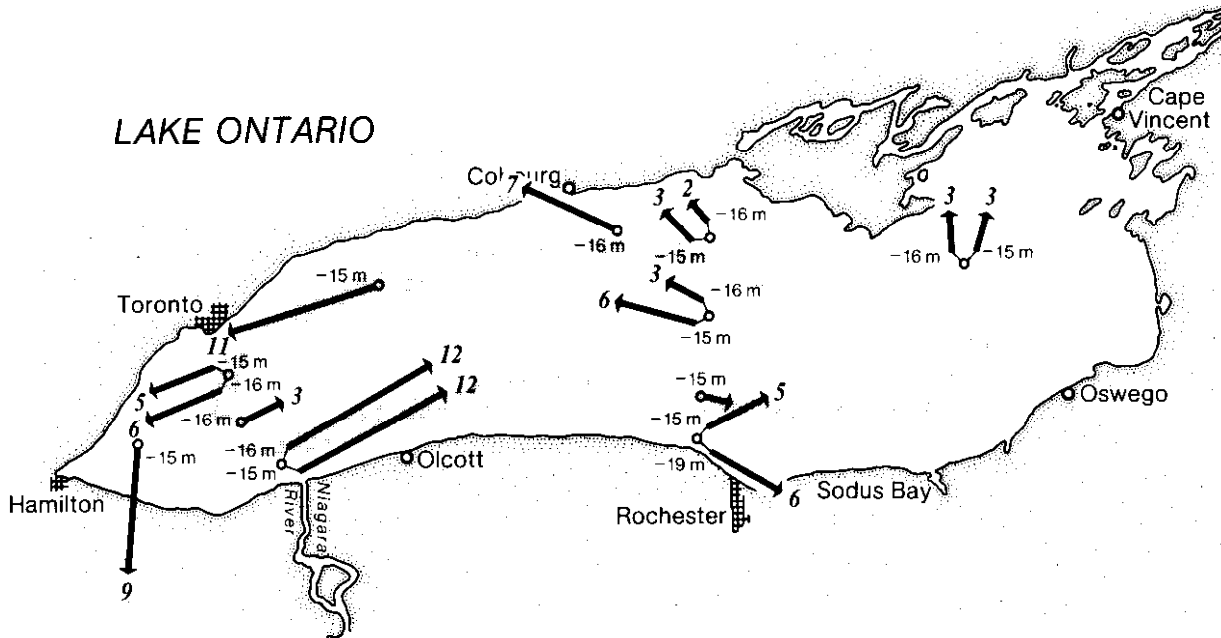# CURRENT VECTOR PLOT LAYER 2

(b)

Figure 11. Layered current vector plots under the northeasterly wind

(a) at 10 m depth

(b) at 30 m depth.

35 m, respectively. The surface layer currents exhibit a dominant cyclonic gyre together with two strong coastal jets congruent to the direction of the wind as indicated in Figure 11a. In the second layer, Figure 11b, the major current is the returning flow against the direction of wind generated mostly by the pressure gradient.

During the IFYGL year, the November wind was from the northeast and had a stress of about 0.5 dyne/cm^2 - the same as the superimposed atmospheric boundary condition for our second demonstration run. The mean November current meter data at 15 m (or 16 m) during IFYGL (Figure 12) has been given by

Lake Ontario November 1972 Observed Currents

Figure 12. November current meter data during IFYGL (from Pickett, 1977).

Pickett (1977). It shows a large cyclonic circulation. All the current meter data, except those from two south shore stations, compare very well in both magnitude and direction with the model currents. The current meter data at the Rochester and Niagara stations showed no symptoms of coastal jets, while the model produced the strong shallow boundary currents along both the north and the south shores. It is probable that the current meter at 15 m (or 16 m) missed the top layer Ekman current near the coast. Again, verification will be discussed in a later report.

6. SUMMARY AND CONCLUSIONS

A time-dependent, three-dimensional numerical dynamic model has been developed for the study of the physical nature and dynamic behavior of the large-scale motion and structure in the lake in response to atmospheric forcing. Two demonstration runs with prevailing monthly winds and heating have

been carried out.   The vertically integrated stream function for the south-
westerly wind, the prevailing wind for July 1972, shows a two-gyre circulation
pattern, a larger anticyclonic gyre in the north and a smaller cyclonic gyre
in the south.   When the prevailing wind blows from the opposite direction to
simulate November 1972 conditions, a similar circulation also emerges, but
the flow directions are reversed.   Surface currents in both cases show strong
coastal jets in the shallow regions and a balancing return flow in the middle.
In the lower layers, return flows opposite to the wind direction are dominant.
Model results compare well with other studies, such as those by Rao and Murty
(1970), Simons (1975), and Baba (1974). However, the simulated current pattern
does not totally agree with the IFYGL data, especially those for July 1972
(Pickett and Richards, 1975).   The discrepancy may be due to the coarse grid
separations in the horizontal and vertical directions without proper resolu-
tion of the boundary layers and the thermocline.   Another probable deficiency
of the present version of the model is the rough approximation of the bottom
topography, which is very important in lake dynamics.   To improve the accuracy
of the model bathymetry, the lowest layer at a computational point is allowed
to have a variable thickness to compensate for the depth difference between
the model layer depth and the actual lake depth.   But, as far as the lake
simulation is concerned, the major concern is for the reliability of the atmos-
pheric boundary conditions, the wind and heat that drive the lake.   The diffi-
culty is even more serious when we are dealing with the monthly mean state.
It is expected that the errors involved with stresses and heating will be
reduced when we carry out time-dependent, seasonal variation runs.   More
simulations, model tuning, and verifications are planned for the near future.

7.   ACKNOWLEDGMENTS

8.   REFERENCES

Arakawa, A. (1966):   Computational design for long-term numerical integration
     of the equations of fluid motion: Two dimensional incompressible flow.
     Part I.   J. *Comput. Phys.*, 1 (1):119-143.

Baba, N. (1974):   A numerical investigation of Lake Ontario: Dynamics and
     thermodynamics.   Ph.D. dissertation, Princeton University, 264 pp.

Bennett, J. R. (1976): A three-dimensional model of Lake Ontario's summer
     circulation.   Submitted to *J.Phys.Oceanogr.*

Bryan, K. (1969):   A numerical method for the study of ocean circulation.
     J. Comput. Phys., 4:347-376.

Businger, J. A., J. C. Wyngaard, Y. Izumi, and E. F. Bradley (1971): Flux-profile relationships in the atmospheric surface layer. J. *Atmos. Sci.*, 28:181-189.

Deardorff, J. W. (1968): Dependence of air-sea transfer coefficients on bulk stability. *J. Geophys. Res.*, 73 (8):2549-2557.

Department of Commerce (1959): Climatology and weather services of the St. Lawrence Seaway and Great Lakes. Weather Bur. Tech. Pap. 35, 75 PP.

Gates, W. L. (1968): A numerical study of transient Rossby waves in a wind-driven homogeneous ocean. *J.Atmos.* Sci., 25:3-22.

Gates, w. L., A. B. Kahle, and E. S. Batten (1971): A documentation of the Mintz-Arakawa two-level atmospheric general circulation model, Report NO. R-877-ARPA, The Rand Corp., Santa Monica, Ca.

Gedney, R. T. and W. Lick (1972): Wind-driven currents in Lake Erie. J. *Geophys. Res.*, 71 (15):2714-2723.

Haney, R. L. (1974): A numerical study of the response of an idealized ocean to large-scale surface heat and momentum flux. *J. Phys. Oceanogr.*, 4 (2):145-167.

Hess, S. L. (1959): *Introduction to Theoretical Meteorology*, Holt, Rinehart and Winston, New York, 355 pp.

Huang, J. C. K. (1973): A multi-layer regional dynamic model of the North Pacific Ocean, Scripps Inst. Oceangr. Sc. Ref. No. 73-23, Scripps Institution of Oceanography, La Jolla, Ca.

Johnson, T. H., G. A. Flittner, and M. W. Cline (1958): Automatic data processing program for marine synoptic radio weather report. Spec. Report 503, Bureau of Comm. Fisheries, 74 pp.

Leendertse, J. J., K. C. Alexander, and S. K. Liu (1973): A three-dimensional model for estuaries and coastal seas: Volume I, Principles of Computation, Report No. R-1417-OWRR, The Rand Corp., Santa Monica, Ca.

Leith, C. E. (1968): Two dimensional eddy viscosity coefficients. In: *Proc. WMO/IUGG Symp.* on *Numer.Weath.Pred.* in *Tokyo*, World Meteorological Organization, pp. 140-144.

Lilly, D. K. (1965): On the computational stability of numerical solutions of time-dependent nonlinear geophysical fluid dynamic problems. Mon. *Weather Rev.*, 93 (1):11-26.

London, J. (1957): A study of the atmospheric heat balance. Final Report, Contract No. AF19 (122)-165, Department of Meteorology and Oceanography, New York University, 99 PP.

Munk, W., and N. Phillips (1968): Coherence and bond structure of inertial motion in the sea. *Rev. of Geophys.*, 6. (4):447-472.

Pandolfo, J. P., and C. A. Jacobs (1972): Numerical simulations of Lake Ontario with a one-dimensional air/lake model. The Center for the Environment and Man, Inc., Hartford, Conn.

Paskausky, D. F. (1971): Winter circulation in Lake Ontario. In: *Proc.,14th Conf. Great Lakes Res.*, International Association for Great Lakes Research, pp. 593-606.

Pickett, R. L., and F. P. Richards (1975): Lake Ontario mean temperatures and currents in July 1972. *J. Phys. Oceanogr.*, 5 (4):775-781.

Pickett, R. L. (1977): The observed winter circulation of Lake Ontario. *J. Phys. Oceanogr.*, 7 (1):153-156.

Platzman, G. W. (1958): A numerical computation of the surge of 26 June 1954 on Lake Michigan. *Geophys.*, 6:407-438.

Platzman, G. W. (1963): The dynamic prediction of wind tides on Lake Erie. *Meteorol. Monogr.*, Vol. 4, No. 26, 44 pp.

Platzman, G. W. (1965): The prediction of surges in the southern basin of Lake Michigan. Part 1: The dynamical basis for prediction. *Mon. Weather Rev.*, 93:275-281.

Rao, D. B., and T. S. Murty (1970): Calculation of the steady state wind-driven circulations in Lake Ontario. *Arch.Met.Geophys.Bioklim.Ser.* A, 19:195-210.

Simons, T. J. (1973): Development of three-dimensional numerical models of the Great Lakes, Canada Centre for Inland Waters Sci. Rept., 85 pp.

Simons, T. J. (1975): Verification of numerical models of Lake Ontario. Part II. Stratified circulations and temperature changes. *J. Phys. Oceanogr.*, 5:98-110.

Vonder-Haar, T. H., and K. J. Hanson (1969): Absorption of solar radiation in tropical regions. *J. Atmos. Sci.*, 26(4):652-655.

9. APPENDIX A.   SYMBOLS AND NOMENCLATURES

A_1, A_2, A_3	cross-sectional areas normal to the equivalent x, y, z axes, respectively
C	Stefan-Boltzman constant
C_H, C_E, C_D	exchange coefficients for heat, water, and momentum, respectively
D	local maximum depth of the lake
e_a	vapor pressure of the air at 10 m above the lake surface (in mb)
f	Coriolis parameter ($2\,\Omega\,\sin\phi$)
N_c	cloudness (in fraction)
p	pressure
p_a	atmospheric pressure at the free surface
p_s	pressure at the balanced lake surface
Q_B	net upward flux of infrared radiation
Q_H	net upward flux of sensible heat
Q_I	downward flux of insolation
Q_E	net upward flux of latent heat
Q_0	solar radiation at the top of the atmosphere
Q_S	net downward heat flux through the air/lake interface
q_a	specific humidity of air at 10 m above lake surface
q_s	saturated humidity
T	temperature
t	time
u	longitudinal velocity component
v	latitudinal velocity component
w	vertical velocity component
z	depth; positive is upward

$$\nabla = \hat{\lambda}\,\frac{\sec\phi}{a}\,\frac{\partial}{\partial\lambda}(\ ) + \hat{\phi}\,\frac{1}{a}\,\frac{\partial}{\partial\phi}(\ )$$

$$\nabla^2 = \hat{\lambda}\,\frac{\sec\phi}{a}\left[\frac{\sec\phi}{a}\,\frac{\partial^2}{\partial\lambda^2}(\ ) + \frac{\partial}{\partial\phi}\,\frac{\cos\phi}{a}\,\frac{\partial}{\partial\phi}(\ )\right]$$

ϕ	latitude
λ	longitude
ρ	density of water
ρ_0	density of water at reference temperature
σ	computational subvolume
τ	surface wind stress
τ_b	bottom stress